

Coherence and flow-maximization of a one-way valve

Andrea Corli*, Ulrich Razafison**, Massimiliano D. Rosini*,***

**Department of Mathematics and Computer Science, University of Ferrara
I-44121 Italy*

***Laboratoire de mathématiques, CNRS UMR 6623, Université de Franche-Comté, 16 route de Gray
25030 Besançon, France*

****Uniwersytet Marii Curie-Skłodowskiej, Plac Marii Curie-Skłodowskiej 1
20-031 Lublin, Poland*

Abstract

We consider a mathematical model for the gas flow through a one-way valve and focus on two issues. First, we propose a way to eliminate the chattering (the fast switch on and off of the valve) by slightly modifying the design of the valve. This mathematically amounts to the construction of a coupling Riemann solver with a suitable stability property, namely, coherence. We provide a numerical comparison of the behavior of the two valves. Second, we analyze, both analytically and numerically, for several significative situations, the maximization of the flow through the modified valve according to a control parameter of the valve and time.

Keywords: systems of conservation laws, gas flow, valve, Riemann problem, coupling conditions, chattering, maximization, control, isentropic Euler equations, p -system.

2010 AMS subject classification: 35L65, 35L67, 76B75

1 Introduction

This paper aims at improving the modeling of a gas flow through a one-way valve, thus carrying on the research on the same subject in [12, 13, 14]. The motivation of these studies is to provide an *analytic* modeling of such flows, which we base on hyperbolic systems of conservation laws and their Riemann solvers. Two related issues are considered here. First, how to remove the chattering (the fast switch on and off) of a valve in correspondence of some threshold states [27, 35], by slightly modifying the design of the valve. Second, the maximization of the flow through the new valve, according to a characteristic parameter of the valve and time.

Since we focus on the behavior of the valve, we make some simplifying assumptions on the flow. The gas flow takes place along two straight pipes having equal and constant cross-sections; the position along the pipes is denoted by $x \in \mathbb{R}$ and they are joint by a valve at $x = 0$. Thus we neglect the wall deformation of the pipes under pressure loads. The flow is characterized by the mass density $\rho > 0$ and the velocity v of the gas; we assume that it is isothermal and so we take

$$p(\rho) \doteq a^2 \rho$$

as pressure law, where the constant $a > 0$ is the sound speed. The flow is governed by the Euler equations

$$\begin{cases} \partial_t \rho + \partial_x(\rho v) = 0, \\ \partial_t(\rho v) + \partial_x(\rho v^2 + p(\rho)) = 0, \end{cases} \quad (1.1)$$

where $t > 0$ is the time. The initial-value problem for system (1.1) when the initial data are constant, apart for a single jump, is called Riemann problem and is well understood [30]. The solution is autosimilar and provided by a *Riemann Solver* \mathcal{RS}_p ; it consists of constant states separated by shock or rarefaction waves. The solver \mathcal{RS}_p satisfies several properties but in particular it is *coherent*; in a few words, this means that, for any solution $u \doteq (\rho, q)$ provided by \mathcal{RS}_p , with $q \doteq \rho v$ being the momentum, the Riemann problem having for initial data the traces $u(t, x^\pm)$ and solved by \mathcal{RS}_p leads to a function having the same local behavior of u in a neighborhood of (t, x) . This property can be understood as a sort of interior stability of \mathcal{RS}_p .

The modeling, maximization, and control of gas flows through networks of pipes have been recently considered in several papers; we refer to [21] for a comprehensive survey on the subject and just quote some relevant references. Among the first papers dealing with a rigorous mathematical modeling of gas flows in networks we quote [4, 5]. There, the authors use system (1.1) and require that only positive velocities are admitted; moreover, at each junction, either the pressure is continuous or the flow is subsonic. We refer to Proposition 2.6 below for a discussion of the latter issue. Then, they find a unique solution under the additional condition that the flow is maximal at each junction. They

also provide some simple numerical modelings of two valves, which have either maximal [4] or zero [5] flux on the outgoing pipe. Optimization and control problems are considered in [3, 20, 22, 25, 26] for gas flows with compressors; in [23, 24, 31] also valves are present, and the problem is solved by suitable discretisations of the modeling equations. We emphasize that in the latter papers the treatment of valves is very different from ours because it is based on the supply and demand functions.

In this paper we pursue the analysis started in [13] and focus again on flow-control valve: roughly speaking, for a fixed flow value q_* , the valve keeps the flow equal to q_* if possible, otherwise it closes. As in [12, 13, 14], the effect of a valve is reproduced by enforcing a coupling between the ingoing and the outgoing flow at $x = 0$. This is encoded by the so-called *coupling Riemann solver*, c-Riemann solver for short, that gives solutions to the Riemann problem at $x = 0$ for (1.1) for the coupling problem induced by the valve. The analysis of coupled Riemann solvers has a long history, starting from the seminal paper [19]; we refer the reader to the recent article [6] for general information and detailed references. We point out, however, that most of the papers in the literature either deal with scalar equations (we consider a system of two equations) or require stricter coupling condition than ours, for example the continuity of the traces at $x = 0$ (in our case this will only hold for the momentum component of the solution). From a mathematical point of view, our modeling rather lies in the framework of constrained Riemann problems: see [11] for scalar conservation laws, [16] for a 2×2 system, and [1] for recent advances. We also point out that, with respect to [4, 5], we neither require the continuity of the pressure nor that flows are subsonic at the valve.

Different valves correspond to different c-Riemann solvers, see [12, 13, 14] and Sections 2, 3 for some examples. A key analytic feature of the modeling is the possible *incoherence* of the corresponding c-Riemann solver, which is related to chattering. Clearly, incoherence leads to the numerical instability of the solution, see for instance the central column in Figure 4.

In this paper we slightly modify the c-Riemann solver \mathcal{RS}_v introduced in [13, Section 4]; the motivation is that \mathcal{RS}_v is incoherent. Incoherent states for \mathcal{RS}_v are supersonic, indeed. In most real gas-flows through pipe networks, supersonic states do not occur, and the reason is attributed to friction terms [4], [33, pages 45 and 49] and safety reasons. Supersonic flows *do* occur in particular circumstances, indeed, see for example [32] and references therein. Moreover, from a mathematical point of view, the invariant domains for the Riemann solver \mathcal{RS}_p always contain supersonic states (see [30]) and, as a consequence, these states can appear even if they are not present initially; the latter happens as well for \mathcal{RS}_v , as we show in Proposition 2.6 (ii). The issue is how to modify \mathcal{RS}_v to recover coherence. The new proposed c-Riemann solver \mathcal{RS}_h

- is coherent;
- differs from \mathcal{RS}_v *only* for the states that lead \mathcal{RS}_v to lose coherence;
- for incoherent initial data, it selects the unique solution that maximizes the flow through the valve among all c-Riemann solvers.

The last property deserves a comment. As it has been first pointed out in [28], such a condition is understood as a sort of “entropy” condition [4, 5, 17, 28], because it singles out solutions uniquely. It is interesting to observe that this property is suggested by the behavior of a valve with a positive reaction time, see Section 3.

We provide some numerical simulations letting us conjecture that \mathcal{RS}_h furnishes the solution obtained by applying \mathcal{RS}_v at every time step Δt (where chattering occurs) as $\Delta t \rightarrow 0$, see the last two columns in Figure 4. We currently miss of a general analytic proof of the latter statement; nevertheless, such simulations suggest that \mathcal{RS}_h reproduces the *final effects* on the gas flow of a chattering valve, without the inconvenient of the (numerical) instability caused by incoherence. This suggests a different design of the valve corresponding to \mathcal{RS}_v , replacing it with the valve corresponding to \mathcal{RS}_h . By the way, the study of the coherence of a constrained Riemann problem is surely of interest from the mathematical point of view.

Here follows an outline of the paper. In Section 2 we first introduce our notation and quickly review some basic facts about system (1.1). We emphasize that, there and in the following, *the Lax curves represented in the pictures are always exact* and not merely qualitative. Then we summarize the modeling of the flow through a valve, with a special focus to the above mentioned valve. Section 3 provides the definition of the modified Riemann solver \mathcal{RS}_h and the proof of its coherence. In Section 4 we first introduce the numerical scheme to be used in the following and the reasons of our choice; then we give some comparisons between exact and numerical solutions. Section 5 is the core of the paper. There, we first state the maximization problem under study; it depends both on the flow threshold q_* and on the time horizon T . In some simple cases the solutions can be computed analytically, and they are compared to the numerical solutions to further validate the numerical scheme. Then we give some numerical simulations of more complicated situations, in particular dealing with the perturbation of the incoming flow of either a shock or a rarefaction.

2 Preliminary results and notation

In this section we first briefly recall the main facts about system (1.1) with the pressure law $p(\rho) = a^2 \rho$, in particular for what concerns Lax curves and their properties. All of them are well known, see [30] and [7, 15] for general information, but this avoids us to systematically refer the reader to other books or papers. Then, we summarize the modeling of a gas flow through a one-way valve [13], which is located at $x = 0$; we also provide some new results.

We always deal with the conservative variables $u \doteq (\rho, q)$, where $q \doteq \rho v$ is the momentum, so that system (1.1) can be written as

$$\begin{cases} \partial_t \rho + \partial_x q = 0, \\ \partial_t q + \partial_x \left(\frac{q^2}{\rho} + a^2 \rho \right) = 0. \end{cases} \quad (2.1)$$

We denote $\Omega \doteq \{(\rho, q) \in \mathbb{R}^2 : \rho > 0\}$. The eigenvalues of (2.1) are $\lambda_1(u) \doteq \frac{q}{\rho} - a$, and $\lambda_2(u) \doteq \frac{q}{\rho} + a$; system (2.1) is strictly hyperbolic in Ω and λ_1, λ_2 are genuinely nonlinear. The Riemann problem for (2.1) is the Cauchy problem with initial condition

$$u(0, x) = \begin{cases} u_\ell & \text{if } x < 0, \\ u_r & \text{if } x \geq 0, \end{cases} \quad (2.2)$$

where $u_\ell, u_r \in \Omega$ are constant states. Solutions to (2.1), (2.2) are meant in the weak sense as follows.

Definition 2.1. A function $u \in \mathbf{C}^0([0, \infty); \mathbf{L}_{\text{loc}}^1(\mathbb{R}; \Omega))$ is a weak solution to the Riemann problem (2.1), (2.2) in $[0, \infty) \times \mathbb{R}$ if for any $\varphi \in \mathbf{C}_c^\infty([0, \infty) \times \mathbb{R}; \mathbb{R})$ we have

$$\begin{aligned} \int_0^\infty \int_{\mathbb{R}} \left[\rho \partial_t \varphi + q \partial_x \varphi \right] dx dt + \rho_\ell \int_{-\infty}^0 \varphi(0, x) dx + \rho_r \int_0^\infty \varphi(0, x) dx &= 0, \\ \int_0^\infty \int_{\mathbb{R}} \left[q \partial_t \varphi + \left(\frac{q^2}{\rho^2} + a^2 \right) \rho \partial_x \varphi \right] dx dt + q_\ell \int_{-\infty}^0 \varphi(0, x) dx + q_r \int_0^\infty \varphi(0, x) dx &= 0. \end{aligned}$$

If $x = \gamma(t)$ is a smooth curve along which a weak solution u is discontinuous, then the following Rankine-Hugoniot conditions must be satisfied, where $u^\pm(t) \doteq u(t, \gamma(t)^\pm)$ are the traces of u along $x = \gamma(t)$:

$$(\rho^+ - \rho^-) \dot{\gamma} = q^+ - q^-, \quad (2.3)$$

$$(q^+ - q^-) \dot{\gamma} = \left(\frac{(q^+)^2}{\rho^+} + a^2 \rho^+ \right) - \left(\frac{(q^-)^2}{\rho^-} + a^2 \rho^- \right). \quad (2.4)$$

For $u_o \in \Omega$ we define $\mathcal{FL}_i^{u_o}, \mathcal{BL}_i^{u_o} : (0, \infty) \rightarrow \mathbb{R}$, $i \in \{1, 2\}$, by

$$\begin{aligned} \mathcal{FL}_1^{u_o}(\rho) &\doteq \begin{cases} \mathcal{R}_1^{u_o}(\rho) & \text{if } \rho \in (0, \rho_o), \\ \mathcal{S}_1^{u_o}(\rho) & \text{if } \rho \in (\rho_o, \infty), \end{cases} & \mathcal{FL}_2^{u_o}(\rho) &\doteq \begin{cases} \mathcal{S}_2^{u_o}(\rho) & \text{if } \rho \in (0, \rho_o), \\ \mathcal{R}_2^{u_o}(\rho) & \text{if } \rho \in [\rho_o, \infty), \end{cases} \\ \mathcal{BL}_1^{u_o}(\rho) &\doteq \begin{cases} \mathcal{S}_1^{u_o}(\rho) & \text{if } \rho \in (0, \rho_o), \\ \mathcal{R}_1^{u_o}(\rho) & \text{if } \rho \in [\rho_o, \infty), \end{cases} & \mathcal{BL}_2^{u_o}(\rho) &\doteq \begin{cases} \mathcal{R}_2^{u_o}(\rho) & \text{if } \rho \in (0, \rho_o), \\ \mathcal{S}_2^{u_o}(\rho) & \text{if } \rho \in (\rho_o, \infty), \end{cases} \end{aligned}$$

where $\mathcal{S}_i^{u_o}, \mathcal{R}_i^{u_o} : (0, \infty) \rightarrow \mathbb{R}$, $i \in \{1, 2\}$, are defined by

$$\mathcal{S}_i^{u_o}(\rho) \doteq \rho \left(\frac{q_o}{\rho_o} + (-1)^i a \left(\sqrt{\frac{\rho}{\rho_o}} - \sqrt{\frac{\rho_o}{\rho}} \right) \right), \quad \mathcal{R}_i^{u_o}(\rho) \doteq \rho \left(\frac{q_o}{\rho_o} + (-1)^i a \ln \left(\frac{\rho}{\rho_o} \right) \right). \quad (2.5)$$

The graphs of the functions $\mathcal{FL}_i^{u_o}$ and $\mathcal{BL}_i^{u_o}$ are the *forward* $\mathbf{FL}_i^{u_o}$ and *backward* $\mathbf{BL}_i^{u_o}$ Lax curves, respectively, of the i -th family through u_o , see Figure 1. Analogously, the shock $\mathcal{S}_i^{u_o}$ and rarefaction $\mathcal{R}_i^{u_o}$ curves through u_o are the graphs of the functions $\mathcal{S}_i^{u_o}$ and $\mathcal{R}_i^{u_o}$. The shock speeds are $s_1^{u_o}(\rho) \doteq v_o - a \sqrt{\rho/\rho_o}$ and $s_2^{u_o}(\rho) \doteq v_o + a \sqrt{\rho/\rho_o}$. A state $(\rho, q) \in \Omega$ is *subsonic* if $|v| < a$ and *supersonic* if $|v| > a$; the *sonic lines* are $q = \pm a \rho$.

We introduce the following notations, see Figure 1 on right for an illustration.

Definition 2.2. For $u_\ell, u_r \in \Omega$ we denote:

- $\bar{u}(u_\ell)$ is the element of $\mathbf{FL}_1^{u_\ell}$ with the maximum q -coordinate;
- $\tilde{u}(u_\ell, u_r)$ is the (unique) element of $\mathbf{FL}_1^{u_\ell} \cap \mathbf{BL}_2^{u_r}$;
- $\hat{u}(q_o, u_\ell)$, for any $q_o \leq \bar{q}(u_\ell)$, is the intersection of $\mathbf{FL}_1^{u_\ell}$ and $q = q_o$ with the largest ρ -coordinate;
- $\tilde{u}(q_o, u_r)$, for any $q_o \geq 0$, is the intersection of $\mathbf{BL}_2^{u_r}$ and $q = q_o$ with the largest ρ -coordinate.

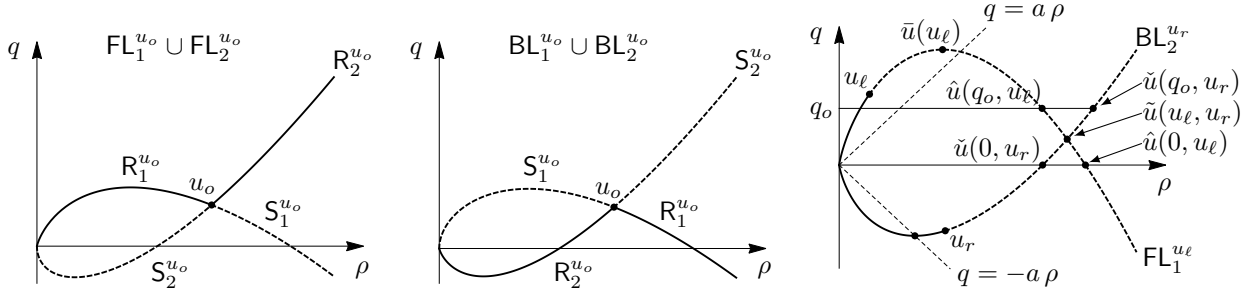


Figure 1: Left: forward Lax curves. Center: backward Lax curves. Right: an illustration of the quantities in Definition 2.2.

Now, we briefly recall the modeling of a gas flow through a *one-way* valve [13]. One-way valves are characterized by letting the flow occur (at $x = 0$) in a single direction; we fix the positive one for definiteness.

We denote by $\mathbf{BV}(\mathbb{R}; \Omega)$ the space of Ω -valued functions with bounded variation. We define $\mathbf{D} \doteq \Omega \times \Omega$. The Lax Riemann solver $\mathcal{RS}_p: \mathbf{D} \rightarrow \mathbf{BV}(\mathbb{R}; \Omega)$, whose action is denoted for $(u_\ell, u_r) \in \mathbf{D}$ by $(t, x) \mapsto \mathcal{RS}_p[u_\ell, u_r](x/t)$, provides the unique entropic solution to Riemann problem (2.1), (2.2), see [30]. We denote for brevity, when the dependence on initial data is clear,

$$u_p \doteq \mathcal{RS}_p[u_\ell, u_r], \quad u_p^\pm \doteq u_p(0^\pm). \quad (2.6)$$

Remark 2.3. *If the 1-wave in u_p is a shock with positive speed, then we have $v_\ell > a$ by (2.5)₁. If the 1-wave is a rarefaction, then it enters the region $x > 0$ if and only if $v_r > a$; if also $a < v_\ell < v_r$, then the whole rarefaction enters the region $x > 0$. An analogous remark holds for 2-waves. As a consequence, subsonic states u_ℓ, u_r never produce waves moving to the same direction.*

Solutions to (2.1) for $x \neq 0$ will always be given by \mathcal{RS}_p ; at $x = 0$ we model the flow through the valve by a *c-Riemann solver* \mathcal{RS} (“c” for coupling), as we are going to define. First, for each $(u_\ell, u_r) \in \mathbf{D}$ we assign the flow $Q = Q(u_\ell, u_r) \in [0, \bar{Q}(u_\ell)]$ through the valve, where $\bar{Q}: \Omega \rightarrow \mathbb{R}$ is given by

$$\bar{Q}(u) \doteq \begin{cases} \bar{q}(u) = \frac{a\rho}{e} \exp\left(\frac{v}{a}\right) & \text{if } v \leq a, \\ q & \text{if } v > a. \end{cases} \quad (2.7)$$

We observe that $\bar{Q} \in \mathbf{C}^1(\Omega)$. The introduction of $\bar{Q}(u)$ is needed to select the values of the flow across the valve, in order that the Riemann solver \mathcal{RS}_c defined below provides at most *one* wave (a 1-rarefaction or a 1-shock) on the left of the valve; see Remark 2.5 (v) below.

Definition 2.4. *Let $Q: \mathbf{D} \rightarrow \mathbb{R}$ be such that $Q(u_\ell, u_r) \in [0, \bar{Q}(u_\ell)]$ for every $(u_\ell, u_r) \in \mathbf{D}$. The corresponding c-Riemann solver $\mathcal{RS}_c: \mathbf{D} \rightarrow \mathbf{BV}(\mathbb{R}; \Omega)$ is defined by*

$$\mathcal{RS}_c[u_\ell, u_r](\xi) \doteq \begin{cases} \mathcal{RS}_p[u_\ell, \hat{u}(Q(u_\ell, u_r), u_\ell)](\xi) & \text{if } \xi < 0, \\ \mathcal{RS}_p[\tilde{u}(Q(u_\ell, u_r), u_r), u_r](\xi) & \text{if } \xi \geq 0. \end{cases} \quad (2.8)$$

Analogously to (2.6) we denote $u_c \doteq \mathcal{RS}_c[u_\ell, u_r]$ and $u_c^\pm \doteq u_c(0^\pm)$.

Remark 2.5. *We now give several explanations of the previous definition and introduce some notations.*

- (i) *A c-Riemann solver \mathcal{RS}_c is characterized by Q . For brevity we omit the dependence on Q .*
- (ii) *The conservation of the mass (which corresponds to the first Rankine-Hugoniot condition (2.3)) must hold at $x = 0$. This condition is automatically satisfied by u_c : if u_c has a stationary discontinuity at $x = 0$, then $\dot{\gamma} = 0$ but $q_c(0^-) = Q(u_\ell, u_r) = q_c(0^+)$ because of the definitions of \tilde{u} and \hat{u} , and so (2.3) holds. On the contrary, the conservation of momentum is lost at $x = 0$, in general; hence the second Rankine-Hugoniot condition (2.4), which encodes this property, cannot be required. Indeed, definition (2.8) does not imply (2.4). As a consequence, u_c may fail to be a weak solution of (2.1) at $x = 0$.*
- (iii) *We say that for $(u_\ell, u_r) \in \mathbf{D}$ the valve is closed if $Q(u_\ell, u_r) = 0$ and open if $Q(u_\ell, u_r) \neq 0$.*
- (iv) *By Definition 2.2 and (2.7) we deduce that $\bar{Q}(u_\ell) \geq q_\ell$ and $0 < \bar{Q}(u_\ell) \leq \bar{q}(u_\ell)$. So, if $Q \in [0, \bar{Q}(u_\ell)]$, then $\hat{u}(Q, u_\ell)$ and $\tilde{u}(Q, u_r)$ are well defined. We denote for short*

$$\hat{u} = \hat{u}(u_\ell, u_r) \doteq \hat{u}(Q(u_\ell, u_r), u_\ell), \quad \tilde{u} = \tilde{u}(u_\ell, u_r) \doteq \tilde{u}(Q(u_\ell, u_r), u_r).$$

By Definition 2.2 we deduce $\hat{\rho} \geq \bar{\rho}(u_\ell)$ and $\hat{q} = Q(u_\ell, u_r) = \bar{q}$.

- (v) *The states $\hat{u} = \hat{u}(u_\ell, u_r)$ and $\tilde{u} = \tilde{u}(u_\ell, u_r)$ are well defined by assuming $Q(u_\ell, u_r) \in [0, \bar{q}(u_\ell)]$. However, it is*

easy to check that the stricter condition $Q(u_\ell, u_r) \leq \bar{Q}(u_\ell)$ required in Definition 2.4 is needed in order that $\xi \mapsto \mathcal{RS}_p[u_\ell, \hat{u}](\xi) \in \text{FL}_1^{u_\ell}$ represents a single wave with negative (≤ 0) speed, and then let (2.8) make sense for $\xi < 0$.

Analogously, condition $Q(u_\ell, u_r) \geq 0$ ensures that $\xi \mapsto \mathcal{RS}_p[\tilde{u}, u_r](\xi) \in \text{FL}_2^{\tilde{u}}$ represents a single wave with positive (≥ 0) speed (so that (2.8) makes sense for $\xi \geq 0$) and it is needed in order that $q(\mathcal{RS}_c[u_\ell, u_r](0)) = q(\mathcal{RS}_p[u_\ell, \hat{u}](0)) = q(\mathcal{RS}_p[\tilde{u}, u_r](0)) \geq 0$.

We now discuss the occurrence of subsonic states for the solver \mathcal{RS}_c .

Proposition 2.6. *Let $(u_\ell, u_r) \in \text{D}$ and $u_c \doteq \mathcal{RS}_c[u_\ell, u_r]$. Then:*

- (i) *The restriction to $\xi < 0$ of u_c attains supersonic values if and only if u_ℓ is supersonic.*
- (ii) *The restriction to $\xi \geq 0$ of u_c may attain supersonic values even if neither u_ℓ nor u_r are supersonic.*

Proof. First, we prove (i). If u_ℓ is subsonic, i.e. $|v_\ell| \leq a$, then $\bar{Q}(u_\ell) = \bar{q}(u_\ell)$ and $\bar{u}(u_\ell)$ is a sonic state by [13, Lemma 2.6]. Therefore for any $\xi < 0$

$$u_c(\xi) = \mathcal{RS}_p[u_\ell, \hat{u}(Q(u_\ell, u_r), u_\ell)](\xi) \in \{u \in \text{FL}_1^{u_\ell} : |v| \leq a\},$$

because by assumption $Q(u_\ell, u_r) \in [0, \bar{Q}(u_\ell)]$. The converse is trivial: if u_ℓ is supersonic, then u_c attains a supersonic value at least at u_ℓ .

About (ii), it is sufficient to choose $Q(u_\ell, u_r)$ sufficiently large in order that $\tilde{u}(Q(u_\ell, u_r), u_r)$ is supersonic. \square

We can now give the definition of a *coherent* coupling Riemann solver.

Definition 2.7. *A c-Riemann solver $\mathcal{RS}_c : \text{D} \rightarrow \text{BV}(\mathbb{R}; \Omega)$ is coherent at $(u_\ell, u_r) \in \text{D}$ if the traces $u_c^\pm \doteq \mathcal{RS}_c[u_\ell, u_r](0^\pm)$ satisfy*

$$\mathcal{RS}_c[u^-, u^+](\xi) = \begin{cases} u_c^- & \text{if } \xi < 0, \\ u_c^+ & \text{if } \xi \geq 0. \end{cases} \quad (2.9)$$

The coherence domain CH of \mathcal{RS}_c is the set of all pairs $(u_\ell, u_r) \in \text{D}$ where \mathcal{RS}_c is coherent. The set $\text{CH}^c \doteq \text{D} \setminus \text{CH}$ is the incoherence domain.

A c-Riemann solver \mathcal{RS}_c is coherent at an initial datum $(u_\ell, u_r) \in \text{D}$ if the ordered pair of the traces of the corresponding solution $(\mathcal{RS}_c[u_\ell, u_r](0^-), \mathcal{RS}_c[u_\ell, u_r](0^+))$ is, in a sense, a fixed point of \mathcal{RS}_c . Hence, coherence may be thought as a stability property. On the contrary, the incoherence of a c-Riemann solver is understood as modeling the chattering of a valve and may yield analytical and numerical instabilities, see for instance the central column in Figure 4.

The Riemann solver \mathcal{RS}_p is coherent in D [12, Proposition 2.5]. On the contrary, coherence may fail for \mathcal{RS}_c because of the presence of a valve. Indeed this is the case for the c-Riemann solver \mathcal{RS}_v introduced in [13] and that we are going to briefly recall. Fix $q_* > 0$, then \mathcal{RS}_v corresponds to the valve that keeps the flow at $x = 0$ equal to q_* if possible, otherwise it closes. This motivates the way $Q = Q_v$ is defined in (2.10) below.

Definition 2.8. *We denote by \mathcal{RS}_v the c-Riemann solver corresponding to*

$$Q_v(u_\ell) \doteq \begin{cases} q_* & \text{if } \bar{Q}(u_\ell) \geq q_*, \\ 0 & \text{if } \bar{Q}(u_\ell) < q_*. \end{cases} \quad (2.10)$$

Notice that Q_v in (2.10) only depends on u_ℓ (and q_* , but for the moment we keep it fixed) and not on u_r . We denote $u_v \doteq \mathcal{RS}_v[u_\ell, u_r]$ and $u_v^\pm \doteq u_v(0^\pm)$. The function Q_v is discontinuous along some curve in Ω ; we explicitly find such a curve in the following Lemma 2.9.

We denote

$$u_*^a \doteq (\rho_*^a, q_*) \doteq (q_*/a, q_*), \quad u_*^0 \doteq (\rho_*^0, 0) \doteq (eq_*/a, 0), \quad (2.11)$$

see Figure 2. Notice that u_*^a is the intersection of the line $\{u \in \Omega : q = q_*\}$ with the sonic line $\{u \in \Omega : v = a\}$. Moreover, u_*^0 is the unique intersection of the curve $\text{BL}_1^{u_*^a}$ with the line $\{u \in \Omega : q = 0\}$.

The following lemma characterizes the states for which the valve is closed; see Figure 2. The function Q_v is then discontinuous along the upper boundary of the set C_ℓ .

Lemma 2.9. *The valve is closed if and only if one of the following equivalent conditions is satisfied:*

- (i) $Q_v(u_\ell) = 0$;
- (ii) $\bar{Q}(u_\ell) < q_*$;
- (iii) u_ℓ belongs to the set

$$\text{C}_\ell \doteq \left((0, \rho_*^a] \times (-\infty, q_*) \right) \cup \left\{ u \in \Omega : \rho > \rho_*^a, q < \mathcal{R}_1^{u_*^a}(\rho) \right\}. \quad (2.12)$$

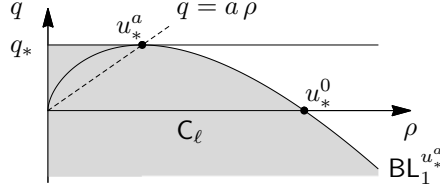


Figure 2: The shaded region represents the set C_ℓ of left states u_ℓ such that the valve corresponding to (2.10) is closed.

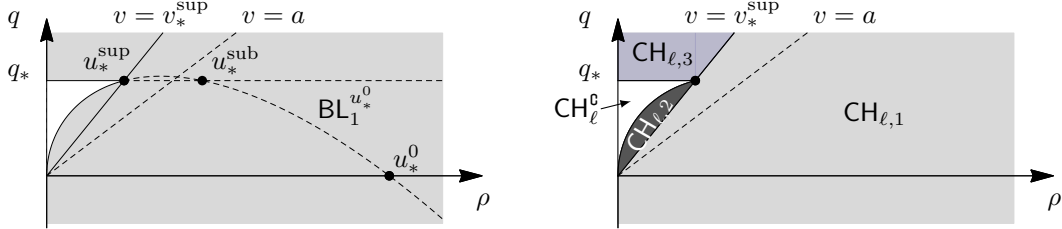


Figure 3: Left: the shaded region represents the coherence domain CH_ℓ , the white region the incoherence domain CH_ℓ^0 . Right: the decomposition of CH_ℓ into the subsets $CH_{\ell,1}$, $CH_{\ell,2}$, $CH_{\ell,3}$ given in (2.15).

We now introduce the states u_*^{sup} and u_*^{sub} , see Figure 3 on the left. Notice that $BL_1^{u_*^0} = S_1^{u_*^0}$ if $q \geq 0$. It is easy to see that the curve $BL_1^{u_*^0}$ intersects the line $q = q_*$ at the two points $u_*^{sup} \doteq (\rho_*^{sup}, q_*)$ and $u_*^{sub} \doteq (\rho_*^{sub}, q_*)$. The state u_*^{sup} is supersonic, the state u_*^{sub} is subsonic with constant speeds

$$v_*^{sup} \approx 1.63 \cdot a, \quad v_*^{sub} \approx 0.81 \cdot a. \quad (2.13)$$

The next theorem characterizes the incoherence domain CH^0 of \mathcal{RS}_v . Since Q_v only depends on the upstream states, it is clear that

$$CH = CH_\ell \times \Omega, \quad CH^0 = CH_\ell^0 \times \Omega,$$

where both $CH_\ell \subseteq \Omega$ and $CH_\ell^0 \doteq \Omega \setminus CH_\ell$ only contain left states u_ℓ .

Theorem 2.10 (Incoherence). *The incoherence domain of \mathcal{RS}_v is $CH^0 = CH_\ell^0 \times \Omega$, where*

$$CH_\ell^0 = \left\{ u \in \Omega : v > v_*^{sup}, S_1^{u_*^0}(\rho) \leq q < q_* \right\}. \quad (2.14)$$

We refer to Figure 3 on the left for a representation of CH_ℓ^0 . By (2.14) we deduce $CH_\ell = CH_{\ell,1} \cup CH_{\ell,2} \cup CH_{\ell,3}$ where, see Figure 3 on the right,

$$CH_{\ell,1} \doteq \left\{ u \in \Omega : v \leq v_*^{sup} \right\}, \quad CH_{\ell,2} \doteq \left\{ u \in \Omega : v > v_*^{sup}, q < S_1^{u_*^0}(\rho) \right\}, \quad CH_{\ell,3} \doteq \left\{ u \in \Omega : v > v_*^{sup}, q \geq q_* \right\}. \quad (2.15)$$

Notice that $CH_{\ell,1}$ is independent of q_* by the definition (2.13) of v_*^{sup} . We now show that if \mathcal{RS}_v is not coherent at (u_ℓ, u_r) then the valve is closed.

Corollary 2.11. *We have $CH_\ell^0 \subseteq C_\ell$ and $\mathcal{RS}_v[CH_\ell^0, \Omega](0^-) \subseteq \Omega \setminus C_\ell \subset CH_\ell$.*

In other words, Corollary 2.11 means that if $(u_\ell, u_r) \in CH^0 = CH_\ell^0 \times \Omega$, then in the solution $u_v = \mathcal{RS}_v[u_\ell, u_r]$ the valve is closed, while in the solution $\mathcal{RS}_v[u_v^-, u_v^+]$ the valve is open and then $(u_v^-, u_v^+) \in CH = CH_\ell \times \Omega$; as a consequence by (2.9) we have $\mathcal{RS}_v[u_v^-, u_v^+](0^\pm) = u_v^\pm$.

3 The coherent c-Riemann solver \mathcal{RS}_h

A drawback of incoherence is that it leads to instabilities. For instance, numerical solutions obtained by exploiting \mathcal{RS}_v at each time step may substantially differ from the *exact* solution u_v in correspondence of incoherent initial data, see for instance the first two columns in Figure 4. This difficulty motivates the design of a new valve, which reproduces the behavior of the valve modeled in Definition 2.8 for coherent initial data but that gives rise to a coherent solver.

We introduce such a valve in Definition 3.1 through its Riemann solver \mathcal{RS}_h (“h” for *coherent*). The solver \mathcal{RS}_h , roughly speaking, is uniquely determined by the following conditions:

- (I) \mathcal{RS}_h is coherent in the whole of $D \doteq \Omega \times \Omega$;

- (II) \mathcal{RS}_h coincides with \mathcal{RS}_v in the coherence region CH of \mathcal{RS}_v ;
- (III) if $(u_\ell, u_r) \in \text{CH}^\circ$, then $\mathcal{RS}_h[u_\ell, u_r]$ maximizes the flow across $x = 0$, that is $q(\mathcal{RS}_h[u_\ell, u_r](0)) \geq q(\mathcal{RS}_c[u_\ell, u_r](0))$ for any c-Riemann solver \mathcal{RS}_c .

As we commented in the Introduction, condition (III) resembles an entropy condition. It has been already exploited in the framework of gas networks, see for instance [4, (28)], [5, (15a)].

Because of (II), the issue is then how to define \mathcal{RS}_h in CH° . A hint comes from [14, §6], where a valve with a reaction time and based on \mathcal{RS}_v is considered. For $(u_\ell, u_r) \in \text{CH}^\circ$, a solution is constructed there by applying a front-tracking algorithm. Rather surprisingly, the reaction time leads to the periodic appearance of a flow q_ℓ at $x = 0$, even if q_ℓ differs from both 0 and q_* .

We are then led to prescribe a new value $Q = Q_h$ of the flow at $x = 0$, which equals q_ℓ in the incoherent region $\text{CH}^\circ = \text{CH}_\ell^\circ \times \Omega$ of \mathcal{RS}_v , see (2.14), and coincides with Q_v in CH , as stated in the following definition.

Definition 3.1. We denote by \mathcal{RS}_h the c-Riemann solver corresponding to

$$Q_h(u_\ell) \doteq \begin{cases} q_* & \text{if } \overline{Q}(u_\ell) \geq q_*, \\ 0 & \text{if } \overline{Q}(u_\ell) < q_* \text{ and } u_\ell \in \text{CH}_\ell, \\ q_\ell & \text{if } u_\ell \in \text{CH}_\ell^\circ, \end{cases} \quad (3.1)$$

where \overline{Q} is defined as in (2.7) and $\text{CH}_\ell^\circ \times \Omega$ is the incoherence domain of \mathcal{RS}_v , see (2.14).

Remark 3.2. Observe that if $\overline{Q}(u_\ell) \geq q_*$ then $u_\ell \in \text{CH}_\ell$, or equivalently, if $u_\ell \in \text{CH}_\ell^\circ$ then $\overline{Q}(u_\ell) < q_*$.

Numerical simulations based on \mathcal{RS}_h reproduce the *same* effect on the gas flow of \mathcal{RS}_v after the chattering, at least in the case considered in Figure 4, see the last two columns. We currently miss of a rigorous proof of this fact.

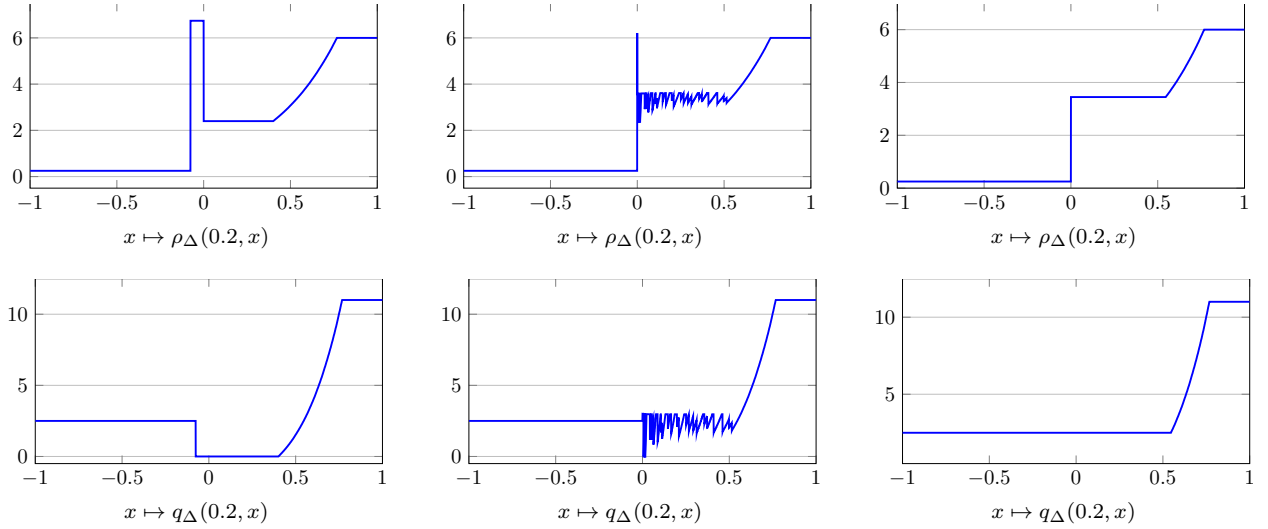


Figure 4: Different numerical simulations for $u(t, x) \doteq \mathcal{RS}_v[u_\ell, u_r](x/t)$. Left column: we computed $Q_v(u_\ell)$ and kept it as flow through the valve for any time. Center column: we applied \mathcal{RS}_v at $x = 0$ at each time step, namely, we updated the flow through the valve according to the left traces of the solution computed at each time step. Right column: $u(t, x) \doteq \mathcal{RS}_h[u_\ell, u_r](x/t)$. Here $\rho_\ell = 0.25$, $q_\ell = 2.5$, $\rho_r = 6$, $q_r = 11$, $a = 2$ and $q_* = 3$, so that $u_\ell \in \text{CH}_\ell^\circ$.

By Corollary 2.11 we have $\text{CH}_\ell^\circ \subset \mathcal{C}_\ell$, hence $\mathcal{C}_\ell^\circ = \text{CH}_\ell \setminus \mathcal{C}_\ell$. This, and Lemma 2.9 (ii), implies

$$\{u_\ell \in \Omega : \overline{Q}(u_\ell) < q_*\} = \mathcal{C}_\ell, \quad \{u_\ell \in \Omega : \overline{Q}(u_\ell) \geq q_*\} = \text{CH}_\ell \setminus \mathcal{C}_\ell, \quad (3.2)$$

and therefore

$$Q_h(u_\ell) = \begin{cases} q_* & \text{if } u_\ell \in \text{CH}_\ell \setminus \mathcal{C}_\ell, \\ 0 & \text{if } u_\ell \in \text{CH}_\ell \cap \mathcal{C}_\ell, \\ q_\ell & \text{if } u_\ell \in \text{CH}_\ell^\circ. \end{cases} \quad (3.3)$$

Now, we collect the main properties of \mathcal{RS}_h . About (III), we notice that it is a consequence of the explicit definition (3.1) and not, as in [4, 5], an implicit consequence of a maximization process.

Proposition 3.3. For any $u_\ell, u_r \in \Omega$ the following holds:

(i) if $(u_\ell, u_r) \in \text{CH}_\ell \times \Omega$, then

$$\mathcal{RS}_h[u_\ell, u_r] \equiv \mathcal{RS}_v[u_\ell, u_r]; \quad (3.4)$$

(ii) if $(u_\ell, u_r) \in \text{CH}_\ell^0 \times \Omega$, then

$$\mathcal{RS}_h[u_\ell, u_r](\xi) = \begin{cases} u_\ell & \text{if } \xi < 0, \\ \mathcal{RS}_p[\tilde{u}(q_\ell, u_r), u_r](\xi) & \text{if } \xi \geq 0, \end{cases} \quad (3.5)$$

and for every c-Riemann solver \mathcal{RS}_c we have

$$q(\mathcal{RS}_c[u_\ell, u_r])(0) \leq q(\mathcal{RS}_h[u_\ell, u_r])(0) \in (0, q_*); \quad (3.6)$$

(iii) \mathcal{RS}_h is coherent in D.

Proof. About (i), formula (3.4) directly follows from Definition 3.1 and by comparing (2.10) with (3.1).

We now prove (ii). About (3.5), if $(u_\ell, u_r) \in \text{CH}_\ell^0 \times \Omega$, then by (2.8) and (3.1) we deduce that

$$\mathcal{RS}_h[u_\ell, u_r](\xi) = \begin{cases} \mathcal{RS}_p[u_\ell, \hat{u}(q_\ell, u_\ell)](\xi) & \text{if } \xi < 0, \\ \mathcal{RS}_p[\tilde{u}(q_\ell, u_r), u_r](\xi) & \text{if } \xi \geq 0. \end{cases}$$

Then, we have two possibilities: either $\hat{u}(q_\ell, u_\ell) = u_\ell$ and so $\mathcal{RS}_p[u_\ell, \hat{u}(q_\ell, u_\ell)] \equiv u_\ell$, or else $\hat{u}(q_\ell, u_\ell) \neq u_\ell$ and so $\mathcal{RS}_p[u_\ell, \hat{u}(q_\ell, u_\ell)]$ consists of constant states u_ℓ and $\hat{u}(q_\ell, u_\ell)$ separated by a stationary shock. In both cases (3.5) immediately follows. To prove (3.6), we first recall (2.8), (3.3) and observe that if $(u_\ell, u_r) \in \text{CH}_\ell^0 \times \Omega$ then

$$q(\mathcal{RS}_h[u_\ell, u_r])(0) = Q_h(u_\ell) = q_\ell.$$

By the definition (2.14) of CH_ℓ^0 we have that both $q_\ell \in (0, q_*)$ and $v_\ell > a$; thus by (2.7) we have

$$q_\ell = \overline{Q}(u_\ell) = \max_{u \in \Omega} q(\mathcal{RS}_p[u_\ell, u])(0) \in (0, q_*).$$

At last, to prove (iii), notice that from (3.5) we have for any $(u_\ell, u_r) \in \text{CH}_\ell^0 \times \Omega$ that

$$\left(\mathcal{RS}_h[u_\ell, u_r](0^-), \mathcal{RS}_h[u_\ell, u_r](0^+) \right) = (u_\ell, \tilde{u}(q_\ell, u_r)) \in \text{CH}_\ell^0 \times \Omega.$$

Moreover $\tilde{u}(q_\ell, \tilde{u}(q_\ell, u_r)) = \tilde{u}(q_\ell, u_r)$ because $q_\ell > 0$, and then \mathcal{RS}_h is coherent in D. \square

Proposition 3.3 proofs the properties of \mathcal{RS}_h listed at the beginning of this section; in particular, formula (3.6) is the maximization of the flow at $x = 0$.

4 Numerical approximation of a c-Riemann solver \mathcal{RS}_c

In this section we introduce the numerical scheme to be used in the following and show some simulations to show its reliability in dealing cases where the valve is involved.

4.1 Description of the numerical scheme

In this subsection, we describe the scheme used to approximate the solutions provided by a given c-Riemann solver \mathcal{RS}_c . It is based on the Random Choice Method (RCM), which was introduced in [18] in order to prove the existence of solutions to systems of non-linear hyperbolic conservation laws. It has then been adapted and used in [9] as a numerical scheme. We also quote [34] and references therein, for the description of the method as a numerical scheme to be implemented.

Let Δx and Δt be the constant space and time steps, respectively. We introduce the points $x_{j+1/2} \doteq j \Delta x$, the cells $K_j \doteq [x_{j-1/2}, x_{j+1/2})$ and the cell centers $x_j \doteq (j - 1/2) \Delta x$ for $j \in \mathbb{Z}$. We denote by j_c the index such that $x_{j_c+1/2}$ is the location of the valve. Define $N \doteq \lfloor T/\Delta t \rfloor$ and, for $n \in \mathbb{Z} \cap [0, N]$, introduce the time discretization $t^n \doteq n \Delta t$. We denote by u_Δ the approximate solution that we assume to be constant in each cell K_j :

$$u_\Delta(t, x) \doteq u_j^n \in \mathbb{R}^2, \quad (t, x) \in [t^n, t^{n+1}) \times K_j.$$

Next, we denote by $\hat{u}_\Delta(Q(u_\ell, u_r), u_\ell)$ and $\tilde{u}_\Delta(Q(u_\ell, u_r), u_r)$ the numerical approximations of $\hat{u}(Q(u_\ell, u_r), u_\ell)$ and $\tilde{u}(Q(u_\ell, u_r), u_r)$, respectively.

The main goal is now to compute u_j^n for any $n \in \mathbb{N} \cap [0, N]$ and $j \in \mathbb{Z}$. We first define

$$u_j^0 \doteq \frac{1}{\Delta x} \int_{K_j} u(0, x) \, dx.$$

Now for a fixed $n \in \mathbb{Z} \cap [0, N]$, assume that u_j^n is given and for any $j \in \mathbb{Z}$. We use the following procedure to compute u_j^{n+1} :

- We pick up randomly or quasi-randomly a number $\theta^n \in [0, 1]$. Here, as in Colella [10] (see also [34]), we consider the van der Corput random sequence (θ^n) defined by

$$\theta^n \doteq \sum_{k=0}^m i_k 2^{-(k+1)},$$

where

$$n \doteq \sum_{k=0}^m i_k 2^k, \quad i_k \in \{0, 1\},$$

denotes the binary expansion of the integer n .

- The updated solution is then computed as follows, for $j \notin \{j_c, j_{c+1}\}$,

$$u_j^{n+1} \doteq \begin{cases} \mathcal{RS}_p \left[u_{j-1}^n, u_j^n \right] (\theta^n \Delta x / \Delta t) & \text{if } 0 \leq \theta^n \leq \frac{1}{2}, \\ \mathcal{RS}_p \left[u_j^n, u_{j+1}^n \right] ((\theta^n - 1) \Delta x / \Delta t) & \text{if } \frac{1}{2} \leq \theta^n \leq 1, \end{cases}$$

and, for $j \in \{j_c, j_{c+1}\}$,

$$u_{j_c}^{n+1} \doteq \begin{cases} \mathcal{RS}_p \left[u_{j_c-1}^n, u_{j_c}^n \right] (\theta^n \Delta x / \Delta t) & \text{if } 0 \leq \theta^n \leq \frac{1}{2}, \\ \mathcal{RS}_p \left[u_{j_c}^n, \hat{u}_\Delta \left(Q(u_{j_c-1}^n, u_{j_c}^n), u_{j_c-1}^n \right) \right] ((\theta^n - 1) \Delta x / \Delta t) & \text{if } \frac{1}{2} \leq \theta^n \leq 1, \end{cases}$$

$$u_{j_{c+1}}^{n+1} \doteq \begin{cases} \mathcal{RS}_p \left[\tilde{u}_\Delta \left(Q(u_{j_c}^n, u_{j_{c+1}}^n), u_{j_{c+1}}^n \right), u_{j_{c+1}}^n \right] (\theta^n \Delta x / \Delta t) & \text{if } 0 \leq \theta^n \leq \frac{1}{2}, \\ \mathcal{RS}_p \left[u_{j_{c+1}}^n, u_{j_{c+2}}^n \right] ((\theta^n - 1) \Delta x / \Delta t) & \text{if } \frac{1}{2} \leq \theta^n \leq 1. \end{cases}$$

Let us note that, as usual, the time steps are chosen with respect to the CFL condition, that is,

$$\Delta t = \frac{C_{\text{cfl}} \Delta x}{\max_{j \in \mathbb{Z}} \max_{i \in \{1, 2\}} |\lambda_i(u_j^n)|},$$

where the CFL coefficient C_{cfl} satisfies $0 \leq C_{\text{cfl}} \leq \frac{1}{2}$. For all the simulations of this paper, we always take $C_{\text{cfl}} = 0.45$.

4.2 Numerical simulations

We use the scheme to compute numerical solutions of some cases involving different configurations of the valve, and we compare them with exact solutions when available. We define the following relative \mathbf{L}^1 -error

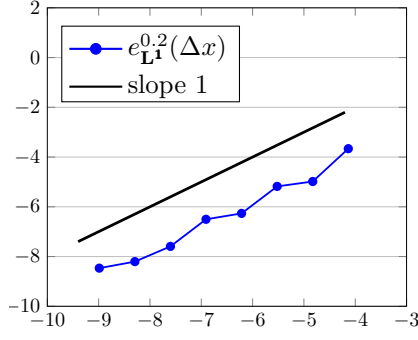
$$e_{\mathbf{L}^1}^t(\Delta x) \doteq \frac{\|u_\Delta(t, \cdot) - u(t, \cdot)\|_{\mathbf{L}^1(I)}}{\|u(t, \cdot)\|_{\mathbf{L}^1(I)}},$$

where $I \subset \mathbb{R}$ is the computational domain. In the remaining part of this subsection, we take

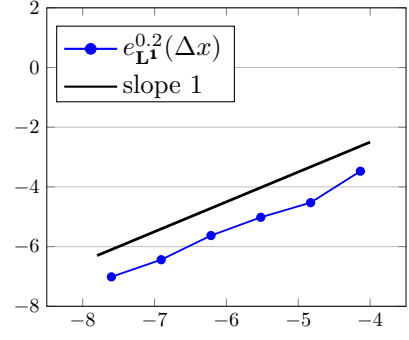
$$I = [-1, 1], \quad a = 2, \quad q_* = 3 \quad \text{and the final time} \quad T = 0.2.$$

In the first two examples, we consider the case where $u_\ell \in \text{CH}_\ell$.

Example 4.1. We take $u_\ell = (6, 1) \in \text{CH}_\ell \setminus \mathbf{C}_\ell$ and $u_r = (1, -1)$. This corresponds to the case when the valve realizes the flow q^* . In Figure 5 (a), we show the numerical convergence of the scheme and this result also shows that the order of convergence is approximately 1. Moreover, we can see in Figures 6 that the numerical solution is in a good agreement with the exact one.



(a) Example 4.1



(b) Example 4.2

Figure 5: Relative \mathbf{L}^1 -errors in log/log scale for Examples 4.1 and 4.2.

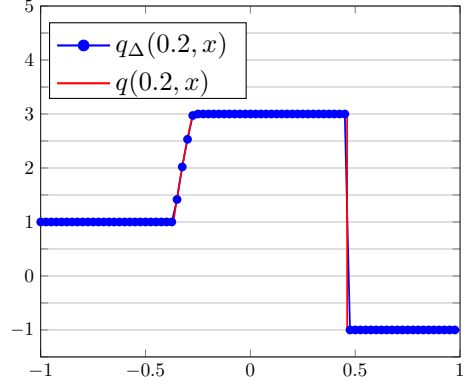
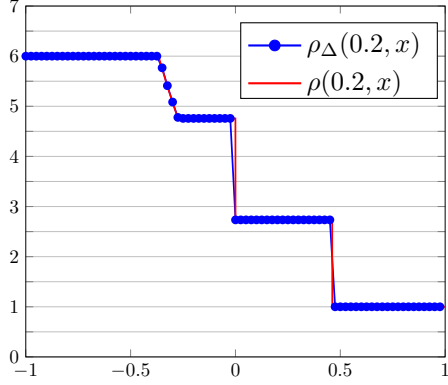


Figure 6: Exact and numerical solutions for Example 4.1 with $\Delta x = 5 \times 10^{-4}$.

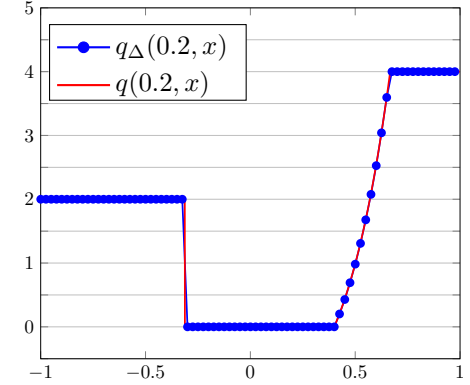
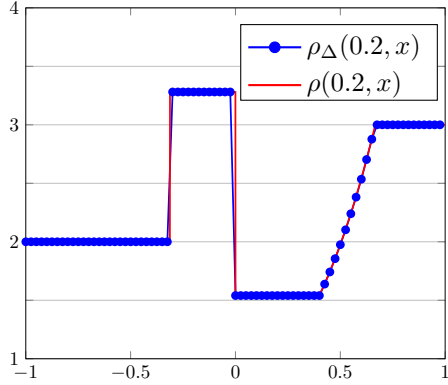


Figure 7: Exact and numerical solutions for Example 4.2 with $\Delta x = 5 \times 10^{-4}$

Example 4.2. We take now $u_\ell = (2, 2) \in \text{CH}_\ell \cap \text{C}_\ell$ and $u_r = (3, 4)$. This corresponds to the case when the valve is closed. As for the previous example, we can see in Figure 5 (b), the numerical convergence of the scheme and that the order of convergence is also approximately 1. Moreover, Figure 7 shows the good agreement between the numerical and the exact solutions.

Remark 4.3. We now provide the main motivation to the choice of the numerical scheme we use in this paper: it lies in the fact that the RCM approximates well single discontinuities. By definition, the state $\tilde{u} = \tilde{u}(Q_h(u_\ell), u_r)$ is given by the intersection of $\text{BL}_2^{u_r}$ and $q = Q_h(u_\ell)$; hence, the solution $\mathcal{RS}_p[\tilde{u}, u_r]$ has a single wave in $\xi > 0$, namely a 2-wave. It is generically impossible, from a numerical point of view, to catch exact values on a curve. For this reason we consider a numerical approximation \tilde{u}_Δ of \tilde{u} . If \tilde{u}_Δ is subsonic, then $\mathcal{RS}_p[\tilde{u}_\Delta, u_r]$ has only a 2-wave in $\xi > 0$ by Remark 2.3. On the contrary, if \tilde{u}_Δ is supersonic, then $\mathcal{RS}_p[\tilde{u}_\Delta, u_r]$ can well have a 1-wave followed by a 2-wave in $\xi > 0$, because Remark 2.3 does not hold any more. Thus essentially any numerical approximation of $\mathcal{RS}_p[\tilde{u}, u_r]$ different from RCM, based on standard finite-volume methods (such as the Godunov scheme) has a 1-wave followed by a 2-wave in $\xi > 0$ if \tilde{u}_Δ is supersonic, by the stability of the scheme. The RCM avoids this severe drawback.

5 Maximization of the flow

In this section we use the solver \mathcal{RS}_h to treat a maximization problem, by looking whenever possible to explicit solutions. Since we let the flow-threshold parameter q_* vary, we use in the following the explicit notation $Q_h^{q_*}$, $C_\ell^{q_*}$, $\text{CH}_\ell^{q_*,0}$ for Q_h , C_ℓ , CH_ℓ^0 given by (3.1), (2.12), (2.14), respectively. As a consequence we denote by $\mathcal{RS}_h^{q_*}$ the c-Riemann solver corresponding to $Q_h^{q_*}$.

We fix a time horizon $T > 0$ and an initial datum attaining the values $u_i, u_\ell, u_r \in \Omega$ (i for “ingoing”) for x belonging to $(-\infty, -1)$, $[-1, 0)$, $[0, \infty)$, respectively; we only let q_* vary. For any $q_* \geq 0$, we denote by $u^{q_*}(t, x) \doteq (\rho^{q_*}(t, x), q^{q_*}(t, x))$ the solution corresponding to the initial condition

$$u^{q_*}(0, x) = \begin{cases} u_i & \text{if } x < -1, \\ u_\ell & \text{if } -1 \leq x < 0, \\ u_r & \text{if } x \geq 0, \end{cases} \quad (5.1)$$

and constructed by applying $\mathcal{RS}_h^{q_*}$ at $x = 0$ and \mathcal{RS}_p elsewhere. The choice of the initial datum as in (5.1) represents a Riemann problem at the valve position with a perturbation on the left. The choice of the point -1 is for simplicity: a different value only leads to a rescaling.

Assume for the moment that for any $q_* \geq 0$ the corresponding solution u^{q_*} is unique and well defined up to a fixed time T . We then study the maximization problem

$$\max_{q_* > 0} \Omega(q_*, T) \quad \text{with} \quad \Omega(q_*, T) \doteq \frac{1}{T} \int_0^T q^{q_*}(t, 0) dt, \quad (5.2)$$

for the average flow $\Omega(q_*, T)$. We point out that the above assumption of existence of solutions is not trivial, because of the possibility of blow up in finite time [2, 8, 29]; furthermore, to solve (5.2) we should also need qualitative properties of the solutions. As a consequence, analytic results for maximization problem (5.2) can hardly be proved in a general setting. For this reason, in the following Subsections 5.1 and 5.2 we focus on some particular cases where *analytical* results are available. These results will be crucial benchmarks for the numerical simulations in Subsections 5.2.2 and 5.2.3, which regard an example which doesn't fit in the analytical results obtained in the preceding subsections. The last Subsection 5.3 contains a further case study which is treated only numerically. For all the numerical simulations performed in the sequel, we always take $\Delta x = 5 \times 10^{-4}$.

5.1 The case $u_i = u_\ell$

In the case $u_i = u_\ell$, problem (5.2) only concerns solutions to a fixed Riemann problem at $x = 0$; in particular, $q^{q_*}(t, 0) = Q_h^{q_*}(u_\ell)$ does not depend on t . We recall that the set $\text{CH}_{\ell,1}$ does not depend on q_* , see (2.15).

Proposition 5.1. *Consider the maximization problem (5.2) in the case $u_i = u_\ell$. Then for any $T > 0$ we have*

$$\max_{q_* > 0} \Omega(q_*, T) = \bar{Q}(u_\ell),$$

and a maximizer is $q_* = \bar{Q}(u_\ell)$. Moreover, the maximizer is unique if and only if $u_\ell \in \text{CH}_{\ell,1}$.

Proof. In the case $u_i = u_\ell$, problem (5.2) reduces to maximize $q_* \mapsto Q_h^{q_*}(u_\ell)$ because $q^{q_*}(t, 0) = Q_h^{q_*}(u_\ell)$ for any $t > 0$ and therefore $\Omega(q_*, T) = Q_h^{q_*}(u_\ell)$ for any $T > 0$.

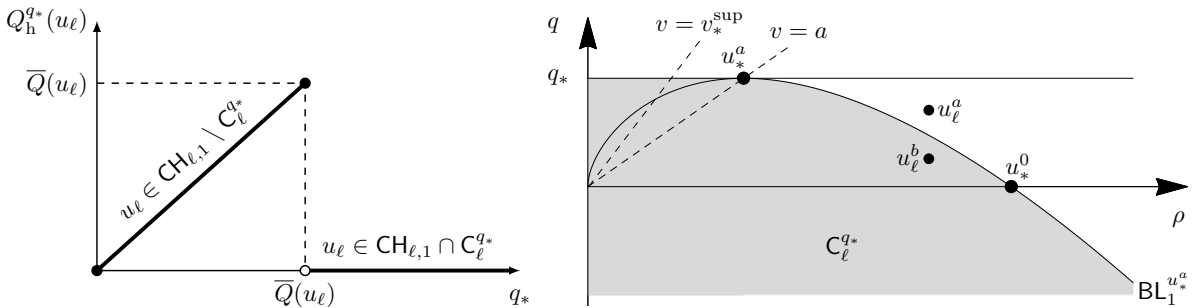


Figure 8: Left: Plot of $q_* \mapsto Q_h^{q_*}(u_\ell)$ with $u_\ell \in \text{CH}_{\ell,1}$ fixed, see (5.3). Right: Two states in $\text{CH}_{\ell,1}$, with $u_\ell^a \in \text{CH}_{\ell,1} \setminus C_\ell^{q_*}$ and $u_\ell^b \in \text{CH}_{\ell,1} \cap C_\ell^{q_*}$. The shaded region represents the set $C_\ell^{q_*}$.

Consider first the case $u_\ell \in \text{CH}_{\ell,1}$, see Figure 8 on the right. By (3.2) and (3.3) we have

$$Q_h^{q_*}(u_\ell) = \begin{cases} q_* & \text{if } q_* \in [0, \bar{Q}(u_\ell)], \\ 0 & \text{if } q_* > \bar{Q}(u_\ell). \end{cases} \quad (5.3)$$

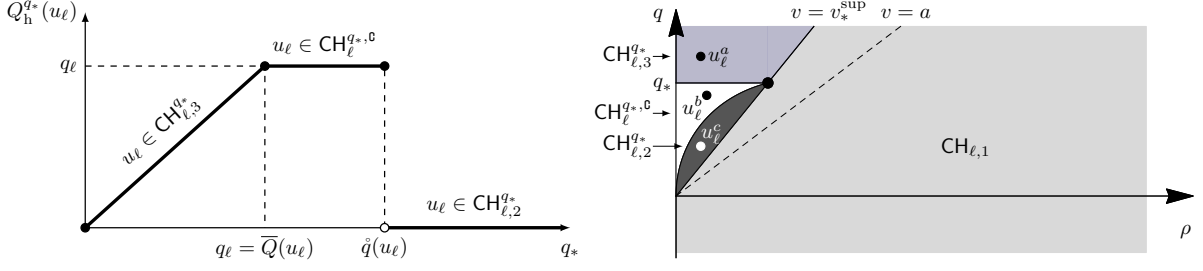


Figure 9: Left: Plot of $q_* \mapsto Q_h^{q_*}(u_\ell)$ with $u_\ell \in \text{CH}_{\ell,1}^0$ fixed, see (5.4). Right: Three possible elements of $\text{CH}_{\ell,1}^0$, with $u_\ell^a \in \text{CH}_{\ell,3}^{q_*}$, $u_\ell^b \in \text{CH}_{\ell,2}^{q_*}$ and $u_\ell^c \in \text{CH}_{\ell,1}^0$.

The plot of $q_* \mapsto Q_h^{q_*}(u_\ell)$ is represented in Figure 8 on the left.

Assume now that $u_\ell \in \text{CH}_{\ell,1}^0$, see Figure 9 on the right. We denote

$$\dot{q}(u) \doteq \bar{q}(\hat{u}(0, u)) = \frac{\rho}{4ae} \left[\sqrt{v^2 + 4a^2} + v \right]^2.$$

Observe that in this case $\bar{Q}(u_\ell) = q_\ell$ by (2.7). We use again (3.3) to deduce the following:

- if $u_\ell \in \text{CH}_{\ell,3}^{q_*} \subset \text{CH}_\ell \setminus \text{C}_\ell$, then we have $Q_h^{q_*}(u_\ell) = q_*$ and $q_* \leq \bar{Q}(u_\ell)$ by (3.2)₂;
- if $u_\ell \in \text{CH}_{\ell,2}^{q_*}$, then we have $Q_h^{q_*}(u_\ell) = q_\ell$ and $q_* \in (\bar{Q}(u_\ell), \dot{q}(u_\ell)]$ by [13, (5.1)];
- if $u_\ell \in \text{CH}_{\ell,1}^0 \subset \text{CH}_\ell \cap \text{C}_\ell$, then we have $Q_h^{q_*}(u_\ell) = 0$ and $q_* > \bar{Q}(u_\ell)$ by (3.2)₁.

Therefore we deduce that

$$Q_h^{q_*}(u_\ell) = \begin{cases} q_* & \text{if } q_* \in [0, \bar{Q}(u_\ell)], \\ q_\ell & \text{if } q_* \in (\bar{Q}(u_\ell), \dot{q}(u_\ell)], \\ 0 & \text{if } q_* > \dot{q}(u_\ell). \end{cases} \quad (5.4)$$

See Figure 9 for the graph of $q_* \mapsto Q_h^{q_*}(u_\ell)$ in this case. This concludes the proof. \square

In Figure 10 we show our numerical simulations corresponding to $a = 2$, $u_r = (1, -1)$ and

$$\text{left:} \quad u_i = u_\ell = (2, 2), \quad \bar{Q}(u_\ell) = \frac{4}{\sqrt{e}} \approx 2.43, \quad (5.5)$$

$$\text{right:} \quad u_i = u_\ell = \left(\frac{1}{4}, \frac{5}{2}\right), \quad \bar{Q}(u_\ell) = \frac{5}{2}, \quad \dot{q}(u_\ell) = \frac{(10 + 2\sqrt{29})^2}{32e} \approx 4.96. \quad (5.6)$$

We notice a very good match with the analytic results, see (5.3) and (5.4). The slight deviation from the expected value 0 (for q_* approximately larger than 5) in Figure 10 on the right is only due to numerical rounding errors.

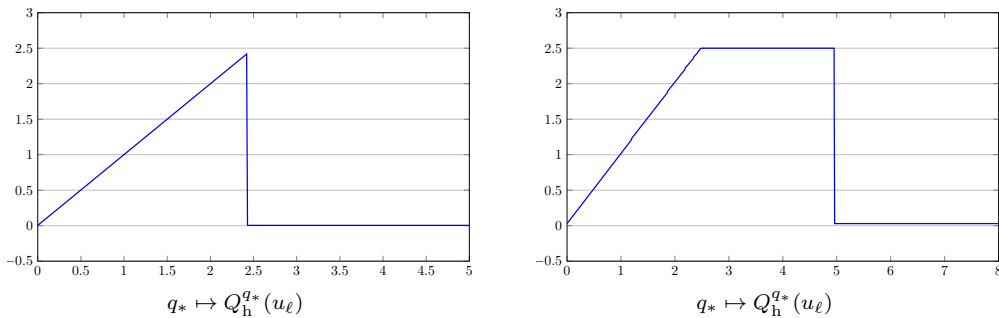


Figure 10: Numerical simulations to the maximization problem (5.2) with $u_i = u_\ell$; the values of the parameters are as in (5.5) and (5.6), respectively.

5.2 The case $\mathcal{RS}_p[u_i, u_\ell]$ is a 2-shock

In this subsection we show how to construct, for small times, an explicit solution to the Cauchy problem for system (2.1) with an initial datum as in (5.1). We apply \mathcal{RS}_p , for $x \neq 0$, and $\mathcal{RS}_h^{q_*}$, at $x = 0$, at each discontinuity of the initial datum and at each wave interaction. As we mentioned above, we focus on a single explicit example; other cases can be handled similarly. We point out that the special case $u_\ell = u_r$ has the advantage of reducing the number

of initial parameters; however, the property $u(t, 0^-) = u(t, 0^+)$ is not preserved when q_* varies, because $\mathcal{RS}_h^{q_*}[u_\ell, u_\ell]$ may lead to solutions that do not have such property. For this reason, we do not treat explicitly this special case.

We assume that at $t = 0$ there is no flow on the right of the valve. On the left, instead, we have a supersonic perturbation u_i which is separated from the state u_ℓ by a 2-shock wave moving toward the valve. For simplicity we assume that the state u_ℓ is sonic. More precisely, see Figure 11, we assume

$$u_\ell \in \text{FL}_2^{u_i}, \quad v_r = 0 < v_\ell = a < v_i, \quad q_r = 0 < q_\ell < \tilde{q}(u_i, \hat{u}(0, u_\ell)) < q_i < \bar{q}(\tilde{u}(u_i, \hat{u}(0, u_\ell))). \quad (5.7)$$

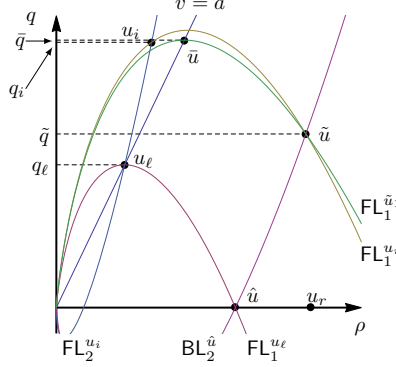


Figure 11: The states u_i , u_ℓ and u_r given in (5.10), (5.12) satisfy (5.7). We denote $\hat{u} \doteq \hat{u}(0, u_\ell)$, $\tilde{u} \doteq \tilde{u}(u_i, \hat{u}(0, u_\ell))$ and $\bar{u} \doteq \bar{u}(\tilde{u}(u_i, \hat{u}(0, u_\ell)))$.

5.2.1 The explicit solution for small times

We now construct an *exact* and *explicit* solution to the initial-value problem (1.1), (5.1) for small times, under the assumptions in (5.7). Since an interaction involving a rarefaction wave is complicate to handle explicitly, we stop the construction when such interactions occur. We distinguish four cases; we emphasize that in the following pictures also the interaction patterns in the space (x, t) (point coordinates and slopes) are *exact* and not merely representative. We refer to Figure 12.

Case (a)

Assume $q_* \in [0, q_\ell]$. For notational simplicity, we denote

$$\hat{u}_1 \doteq \hat{u}(q_*, u_\ell), \quad \tilde{u}_1 \doteq \tilde{u}(q_*, u_r), \quad \tilde{u}_1 \doteq \tilde{u}(u_i, \hat{u}_1), \quad \hat{u}_2 \doteq \hat{u}(q_*, \tilde{u}_1), \quad \tilde{u}_2 \doteq \tilde{u}(u_i, \hat{u}_2). \quad (5.8)$$

At time $t = 0$ a 2-shock with positive speed $s_2^{u_i}(\rho_\ell)$ starts from $x = -1$; a 1-shock with negative speed $s_1^{u_\ell}(\hat{\rho}_1)$, a stationary non-classical shock and a 2-shock with positive speed $s_2^{\tilde{u}_1}(\rho_r)$ are generated at $x = 0$. The first two shocks interact at time $t_1 > 0$ in $x = x_1 < 0$: a 1-shock with speed $s_1^{\tilde{u}_1}(\hat{\rho}_1)$ and a 2-shock with positive speed $s_2^{\tilde{u}_1}(\hat{\rho}_1)$ are generated. The latter shock eventually reaches $x = 0$ at time t_2 . By applying $\mathcal{RS}_h[\tilde{u}_1, \tilde{u}_1]$, we deduce that a 1-shock with negative speed $s_1^{\tilde{u}_1}(\hat{\rho}_2)$ and a stationary non-classical shock start from $x = 0$ at time t_2 ; the former shock eventually interacts at time t_3 and position x_3 with the 1-shock that was generated at time t_1 . As a result of such interaction, a 1-shock with negative speed $s_1^{u_\ell}(\hat{\rho}_2)$ and a 2-rarefaction with positive speeds ranging in $[\lambda_2(\tilde{u}_2), \lambda_2(\hat{u}_2)]$ start from $x = x_3$ at time t_3 . Because a rarefaction showed up, we stop the construction as soon as it reaches the valve; we denote such a time by $T_a^{q_*}$. Notice that the low value of q_* lets the valve open already at $t = 0^+ \doteq$ with flow q_* on the right; the valve keeps open and the flow is q_* at least until time $T_a^{q_*}$.

Case (b)

Assume $q_* \in (q_\ell, \tilde{q}(u_i, \hat{u}(0, u_\ell))]$. We still use notation (5.8) with the exception of $\hat{u}_1 \doteq \hat{u}(0, u_\ell)$. As in the previous case, at time $t = 0$ a 2-shock with positive speed $s_2^{u_i}(\rho_\ell)$ starts from $x = -1$; however, because of the larger value of q_* , only a 1-shock with negative speed $s_1^{u_\ell}(\hat{\rho}_1)$ and a stationary non-classical shock are generated at $x = 0$, and the valve is closed. At time $t_1 > 0$ the two classical shocks interact at $x = x_1 < 0$: a 1-shock with speed $s_1^{\tilde{u}_1}(\hat{\rho}_1)$ and a 2-shock with positive speed $s_2^{\tilde{u}_1}(\hat{\rho}_1)$ are generated. The latter shock eventually reaches $x = 0$ at time t_2 . By considering $\mathcal{RS}_h[\tilde{u}_1, u_r]$, we deduce that a 1-shock with negative speed $s_1^{\tilde{u}_1}(\hat{\rho}_2)$, a stationary non-classical shock and a 2-shock with positive speed $s_2^{\tilde{u}_1}(\rho_r)$ leave $x = 0$ at time t_2 . Roughly speaking, the effect of the supersonic perturbation is not much damped by the shock from $x = 0$ and opens the valve. The new 1-shock eventually interacts at time t_3 and position x_3 with the 1-shock appeared at time t_1 : a 1-shock with negative speed $s_1^{u_\ell}(\hat{\rho}_2)$ and a 2-rarefaction with positive speeds ranging in $[\lambda_2(\tilde{u}_2), \lambda_2(\hat{u}_2)]$ are generated. Then we stop the construction at time $T_b^{q_*}$ when the above 2-rarefaction reaches $x = 0$.

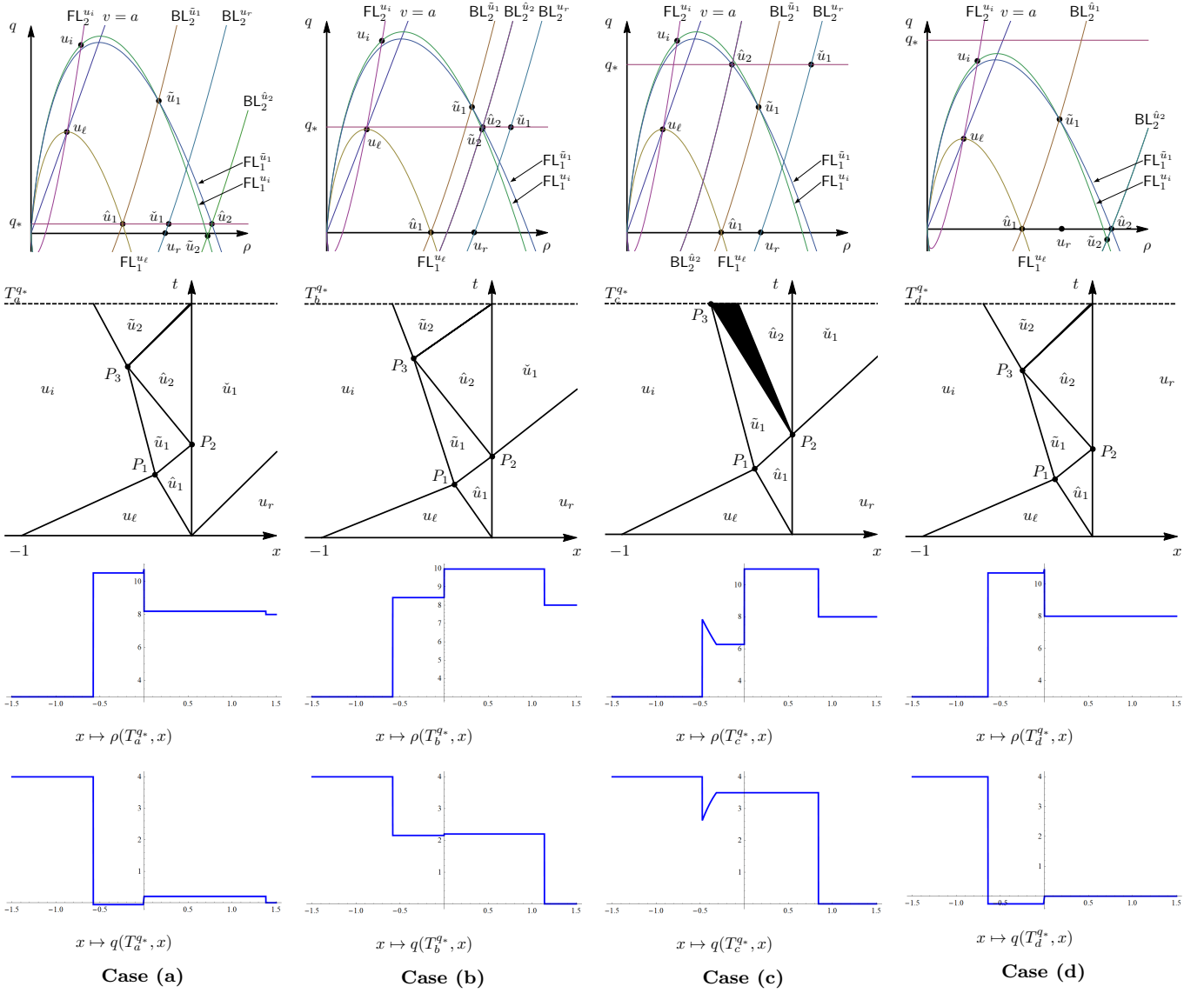


Figure 12: Cases considered in Subsection 5.2.1. Notation is as in (5.8) and in the text. The values of the involved states are listed at the end of Subsection 5.2.1.

Case (c)

Assume $q_* \in (\bar{q}(u_i, \hat{u}(0, u_\ell)), \bar{q}(\tilde{u}(u_i, \hat{u}(0, u_\ell)))$. In this case and in the following one we omit some details, which are as in the two previous cases. Here, differently from **Case (b)**, from P_2 a 1-rarefaction appears on the left of $x = 0$. This is a consequence of the higher value of q_* , which lets more flow pass to the right. Then we stop the construction at time T_c^{q*} when such 1-rarefaction interacts with the 1-shock created at time t_1 .

Case (d)

Assume $q_* > \bar{q}(\tilde{u}(u_i, \hat{u}(0, u_\ell)))$. The construction is analogous to that in **Case (b)**. The only differences are that $\hat{u}_2 \doteq \hat{u}(0, \tilde{u}_1)$ and until time t_3 the valve is closed, so that no waves appear in $x > 0$. Notice that the very high value of q_* lets the valve closed at least until time T_d^{q*} when a 2-rarefaction reaches $x = 0$.

Notice now that in **Case (a)** the points P_1, P_2, P_3 coalesce to the point P_* as $q_* \nearrow q_\ell$, where $P_* = (0, s_2^{u_i}(\rho_\ell)^{-1})$ is the intersection of the t -axis and the line passing through the point $(-1, 0)$ with slope $s_2^{u_i}(\rho_\ell)^{-1}$, that is the line passing through $(-1, 0)$ and P_1 in Figure 12. Hence, by comparing the above constructions, see again Figure 12, it is now clear that the smallest time T which allows an explicit construction of the solution for any $q_* \geq 0$ is precisely

$$T = T_{\min} \doteq \min\{T_a, T_b, T_c, T_d\} = s_2^{u_i}(\rho_\ell)^{-1}. \quad (5.9)$$

where

$$\begin{aligned} T_a &\doteq \min\{T_a^{q*} : q_* \in [0, q_\ell]\}, \\ T_b &\doteq \inf\{T_b^{q*} : q_* \in (q_\ell, \bar{q}(u_i, \hat{u}(0, u_\ell)))\}, \\ T_c &\doteq \inf\{T_c^{q*} : q_* \in (\bar{q}(u_i, \hat{u}(0, u_\ell)), \bar{q}(\tilde{u}(u_i, \hat{u}(0, u_\ell))))\}, \\ T_d &\doteq \inf\{T_d^{q*} : q_* > \bar{q}(\tilde{u}(u_i, \hat{u}(0, u_\ell)))\}. \end{aligned}$$

Then it is easy to see that

$$\max_{q^* > 0} \mathfrak{Q}(q^*, T) = \overline{Q}(u_\ell) = q_\ell,$$

and the unique maximizer is $q_* = \overline{Q}(u_\ell) = q_\ell$. In other words, the choice of reducing the maximization process only to times prior to the first interaction involving a rarefaction leads to the same result of Subsection 5.1 for the Riemann problem, even if the construction is different.

In Subsections 5.2.2 and 5.2.3 we numerically investigate two cases: $u_i \in \text{CH}_{\ell,1}$ and $u_i \in \text{CH}_{\ell,1}^c$, respectively. The differences between these two cases are highlighted by comparison of Figures 14 and 16.

5.2.2 A numerical solution of the maximization problem in the case $v_i < v_*^{\text{sup}}$

It is not easy to tackle the maximization problem (5.2) from an analytic point of view, even under condition (5.7) and for short times. We provide instead a numerical simulation.

We begin by plotting the numerical solutions of Subsection 5.2.1 for specific values. The states in Figure 11 and the exact solutions constructed in Figure 12 are represented below by taking

$$a = 1, \quad \rho_i = 3, \quad q_i = 4, \quad \rho_r = 8, \quad q_r = 0, \quad (5.10)$$

and the following values of q_* for the corresponding cases

$$q_*^a = 0.2, \quad q_*^b = 2.2, \quad q_*^c = 3.5, \quad q_*^d = 4.5. \quad (5.11)$$

Notice that $v_i = q_i/\rho_i = 4/3 \approx 1.33 > 1 = a$, and then v_i is supersonic; however $v_i < 1.63 = v_*^{\text{sup}}$. Notice moreover that the above construction and the choice in (5.10) lead to

$$\rho_\ell \approx 2.15, \quad v_\ell = 1, \quad q_\ell \approx 2.15, \quad (5.12)$$

$$\hat{\rho}(0, u_\ell) \approx 5.64, \quad v_i = 4/3, \quad \tilde{q}(u_i, \hat{u}(0, u_\ell)) \approx 2.62, \quad (5.13)$$

$$\tilde{\rho}(u_i, \hat{u}(0, u_\ell)) \approx 7.85, \quad v_r = 0, \quad \bar{q}(u_i, \hat{u}(0, u_\ell)) \approx 4.03, \quad (5.14)$$

while by (5.11) and (5.9) we have

$$T_a^{q_*^a} \approx 1.37, \quad T_b^{q_*^b} \approx 1.56, \quad T_c^{q_*^c} \approx 1.26, \quad T_d^{q_*^d} \approx 1.44, \quad T_{\min} \approx 0.46. \quad (5.15)$$

In particular, the conditions listed in (5.7) are satisfied, see Figure 11, and $q_*^a < q_\ell < q_*^b < \tilde{q}(u_i, \hat{u}(0, u_\ell)) < q_*^c < \bar{q}(u_i, \hat{u}(0, u_\ell)) < q_*^d$. In Figure 13 we show the outputs of our numerical simulations, which highlight a very good match with the exact solution and confirm the validity of the numerical scheme. Notice, both in **Case (a)** and **Case (d)**, the persistence of a negative left flow from the valve, as it was indeed forecast by the top pictures in Figure 12.

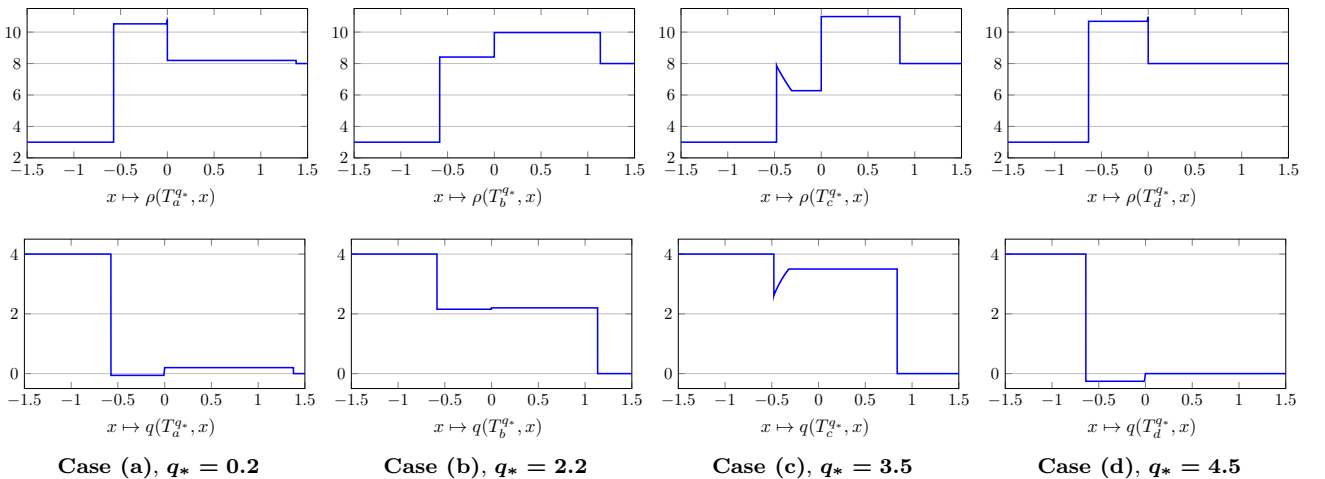


Figure 13: Numerical simulations of the cases in Subsection 5.2.1 and corresponding to the values listed in (5.10), (5.12). The spikes in the ρ -profiles for the first and last case appear also in the exact solutions and correspond to a 2-rarefaction followed by a non-classical stationary shock at $x = 0$.

In Figure 14, we show the numerical result obtained with the same values as in (5.10), (5.12) and $T = 2 > T_{\min}$, see (5.15). Recall that even at time $T = 2$ an exact expression of the solution is not easily available. We notice, in Figure 14, that the function $q_* \mapsto \mathfrak{Q}(q_*, T)$ has up to two discontinuities, which can be interpreted as follows:

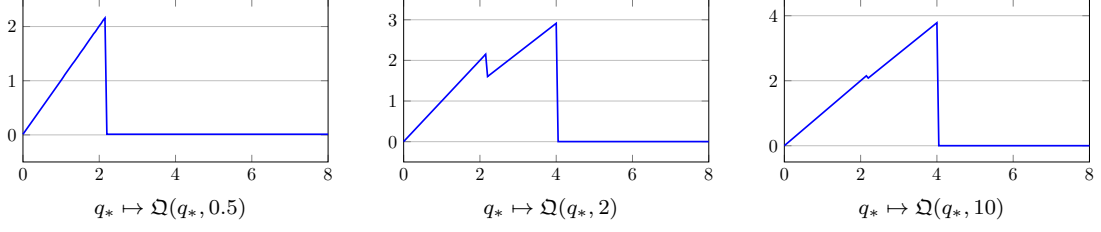


Figure 14: Numerical simulations corresponding to the values in (5.10), (5.12) and for different values of T .

- if $q_* \in [0, q_\ell]$, then for any $t \geq 0$ we have $u^{q_*}(t, 0^-) \in \Omega \setminus \mathcal{C}_\ell^{q_*}$ and therefore $q^{q_*}(t, 0) = q_*$;
- if $q_* \in (q_\ell, \bar{q}(\tilde{u}(u_i, \hat{u}(0, u_\ell))))$, then for any $t \in [0, t_2]$ we have $u^{q_*}(t, 0^-) \in \mathcal{C}_\ell^{q_*} \cap \mathcal{CH}_\ell^{q_*}$ and therefore $q^{q_*}(t, 0) = 0$, whereas for any $t \geq t_2$ we have $u^{q_*}(t, 0^-) \in \Omega \setminus \mathcal{C}_\ell^{q_*}$ and therefore $q^{q_*}(t, 0) = q_*$;
- if $q_* > \bar{q}(\tilde{u}(u_i, \hat{u}(0, u_\ell)))$, then for any $t \geq 0$ we have $u^{q_*}(t, 0^-) \in \mathcal{C}_\ell^{q_*} \cap \mathcal{CH}_\ell^{q_*}$ and therefore $q^{q_*}(t, 0) = 0$.

As a further check of the simulations, we plotted in Figure 15 the numerical traces $u_\Delta^{q_*}(t, 0^-)$, $t \in (0, T]$, for the four different values of q_* listed in (5.11). As a consequence, for $T \in [0, 2]$ the solution of the maximization problem (5.2)

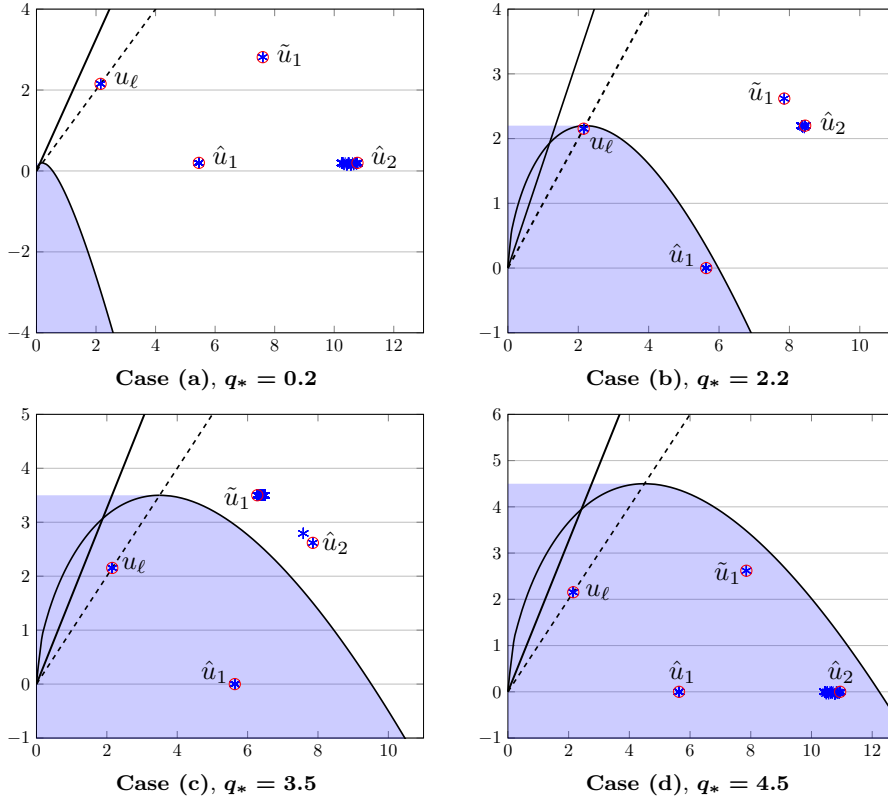


Figure 15: Representation in the (ρ, q) -phase plane of the left traces at $x = 0$ of the solutions constructed in Subsections 5.2.1 and 5.2.2, and corresponding to the values listed in (5.10), (5.12). The stars correspond to the values obtained numerically for $t \in (0, 2]$, while the circles correspond to the exact values for t respectively in $[0, T_a^{q_*}]$, $[0, T_b^{q_*}]$, $[0, T_c^{q_*}]$ and $[0, T_d^{q_*}]$. The curves correspond to $\mathcal{BL}_1^{u_*}$, the shaded regions to $\mathcal{C}_\ell^{q_*}$, the solid lines to $q = v_*^{\text{sup}} \rho$ and the dashed lines to $q = a \rho$, see (2.11), (2.12) and (2.13). Notice that the traces u_ℓ and \tilde{u}_1 are attained only at times $t = 0$ and $t = t_2$, respectively.

is

$$\mathfrak{Q}(q_*, T) = \begin{cases} q_* & \text{for } q_* \in [0, q_\ell] \text{ and } T > 0, \\ 0 & \text{for } q_* \in (q_\ell, \bar{q}(\tilde{u}(u_i, \hat{u}(0, u_\ell)))) \text{ and } T \in [0, t_2], \\ \frac{T-t_2}{T} q_* & \text{for } q_* \in (q_\ell, \bar{q}(\tilde{u}(u_i, \hat{u}(0, u_\ell)))) \text{ and } T > t_2, \\ 0 & \text{for } q_* > \bar{q}(\tilde{u}(u_i, \hat{u}(0, u_\ell))) \text{ and } T > 0, \end{cases} \quad (5.16)$$

where $t_2 \approx 0.54$ corresponds to P_2 in Figure 12, **Case (b)** and **Case (c)**. We observe that Figure 14 highlights a good match with the expression in (5.16) of $\mathfrak{Q}(q_*, 2)$, see (5.12), (5.13) and (5.14).

5.2.3 A numerical solution of the maximization problem in the case $v_i > v_*^{\sup}$

In this subsection we consider the case when $v_i > v_*^{\sup} \approx 1.63 \cdot a$. The analytic construction is similar to the one performed in Subsection 5.2.1 (which mainly aimed at checking the validity of the numerical scheme), so we do not repeat it. We guess that u_i will reach the valve for T sufficiently large. In this case Figure 14 will be different/richer, see Figure 16, and we can comment it and point out the new features.

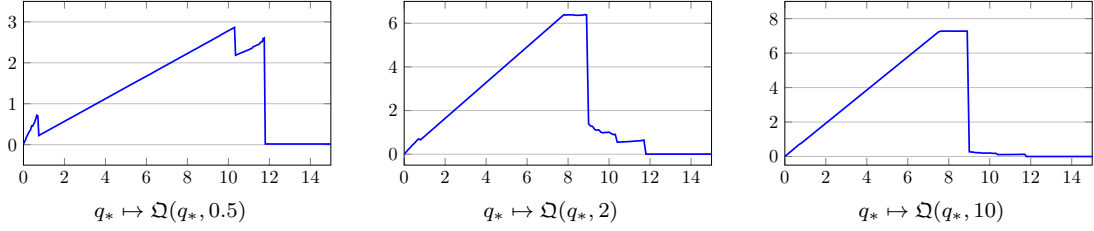


Figure 16: Numerical simulations corresponding to (5.17), (5.18) and for different values of T .

In order to have the same wave structure outlined at the beginning of Section 5.2 (namely, a supersonic perturbation u_i which is separated from the state u_ℓ by a 2-shock wave moving toward the valve) we now replace (5.10) with

$$a = 1, \quad \rho_i = 3, \quad q_i = 7.5, \quad \rho_r = 8, \quad q_r = 0, \quad (5.17)$$

which lead to

$$\rho_\ell \approx 0.75, \quad v_\ell = 1, \quad q_\ell \approx 0.75, \quad \rho_r \approx 8 \quad (5.18)$$

Notice that $v_i = 2.5 \cdot a > v_*^{\sup} \approx 1.63 \cdot a$. The last picture in Figure 16 resembles the last picture in Figure 10. This is probably due to the fact that the solution corresponding to the initial datum (5.1) with u_i , u_ℓ and u_r given by (5.17), (5.18) converges for $t \rightarrow \infty$ to the solution of the Riemann problem corresponding to the states u_i and u_r .

5.3 The case $\mathcal{RS}_p[u_i, u_\ell]$ is a 2-rarefaction

In this final subsection we pursue the analysis of a perturbation interacting with the valve from the left, that we began in Subsection 5.2 with the case of a 2-shock wave, by considering the case of a 2-rarefaction wave. In this case, as we mentioned above, analytically computations are too heavy to be provided, and therefore we focus on numerical simulations. More precisely we consider the data

$$a = 1, \quad \rho_i = 3, \quad q_i = 0, \quad \rho_\ell \approx 8.15, \quad q_\ell \approx 8.15, \quad \rho_r = 8, \quad q_r = 0, \quad (5.19)$$

Notice that the values of a , ρ_i , ρ_r and q_r are as in (5.10) and (5.17). The following Figure 17 shows our numerical simulations, and has to be compared with Figures 14 and 16. We notice a similar behavior of the function $\mathcal{Q}(q_*, T)$, which is interpreted as in the previous case, see (5.16).

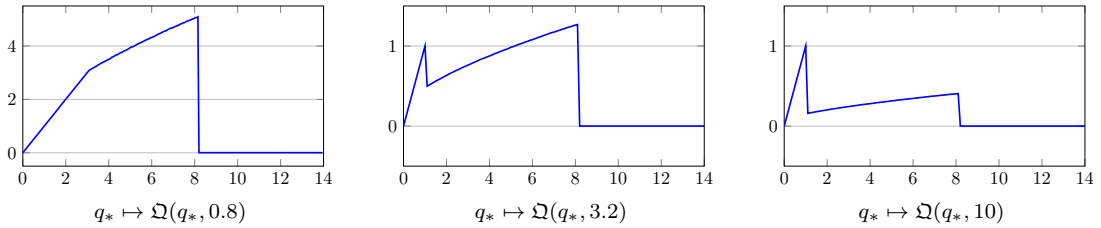


Figure 17: Numerical simulations corresponding to (5.19) for different values of T .

Acknowledgment

A. Corli and M.D. Rosini are members of the *Gruppo Nazionale per l'Analisi Matematica, la Probabilità e le loro Applicazioni* (GNAMPA) of the *Istituto Nazionale di Alta Matematica* (INdAM) and acknowledge financial support from this institution. The second author acknowledges the support of the Région Bourgogne Franche-Comté, projet 2017–2020 “Analyse mathématique et simulation numérique d’EDP issus de problèmes de contrôle et du trafic routier”, and Instytut Matematyki, Uniwersytet Marii Curie-Skłodowskiej, and Dipartimento di Matematica e Informatica, Università degli Studi di Ferrara for the hospitality during the preparation of the paper. The last author acknowledges the support of the National Science Centre, Poland, Project “Mathematics of multi-scale approaches in life and social sciences” No. 2017/25/B/ST1/00051 and by University of Ferrara, FIR Project 2019 “Leggi di conservazione di tipo iperbolico: teoria ed applicazioni”.

References

- [1] B. Andreianov, C. Donadello, U. Razafison, and M. D. Rosini. One-dimensional conservation laws with nonlocal point constraints on the flux. In *Crowd dynamics. Vol. 1*, Model. Simul. Sci. Eng. Technol., pages 103–135. Birkhäuser/Springer, Cham, 2018.
- [2] P. Baiti and H. K. Jenssen. Blowup in L^∞ for a class of genuinely nonlinear hyperbolic systems of conservation laws. *Discrete Contin. Dynam. Systems*, 7(4):837–853, 2001.
- [3] M. K. Banda and M. Herty. Towards a space mapping approach to dynamic compressor optimization of gas networks. *Optimal Control Appl. Methods*, 32(3):253–269, 2011.
- [4] M. K. Banda, M. Herty, and A. Klar. Coupling conditions for gas networks governed by the isothermal Euler equations. *Netw. Heterog. Media*, 1(2):295–314, 2006.
- [5] M. K. Banda, M. Herty, and A. Klar. Gas flow in pipeline networks. *Netw. Heterog. Media*, 1(1):41–56, 2006.
- [6] B. Boutin, F. Coquel, and P. G. LeFloch. Coupling techniques for nonlinear hyperbolic equations. II. Resonant interfaces with internal structure. *Preprint*, 2021.
- [7] A. Bressan. *Hyperbolic systems of conservation laws*, volume 20. Oxford University Press, Oxford, 2000.
- [8] A. Bressan, G. Chen, Q. Zhang, and S. Zhu. No BV bounds for approximate solutions to p -system with general pressure law. *J. Hyperbolic Differ. Equ.*, 12(4):799–816, 2015.
- [9] A. J. Chorin. Random choice solution of hyperbolic systems. *J. Comput. Phys.*, 22(4):517–533, 1976.
- [10] P. Colella. Glimm’s method for gas dynamics. *SIAM J. Sci. Statist. Comput.*, 3(1):76–110, 1982.
- [11] R. M. Colombo and P. Goatin. A well posed conservation law with a variable unilateral constraint. *J. Differential Equations*, 234(2):654–675, 2007.
- [12] A. Corli, M. Figiel, A. Futa, and M. D. Rosini. Coupling conditions for isothermal gas flow and applications to valves. *Nonlinear Anal. Real World Appl.*, 40:403–427, 2018.
- [13] A. Corli and M. D. Rosini. Coherence and chattering of a one-way valve. *ZAMM Z. Angew. Math. Mech.*, 99(6):e201800250, 25, 2019.
- [14] A. Corli and M. D. Rosini. Coherence of coupling Riemann solvers for gas flows through flux-maximizing valves. *SIAM J. Appl. Math.*, 79(6):2593–2614, 2019.
- [15] C. M. Dafermos. *Hyperbolic conservation laws in continuum physics*. Springer-Verlag, Berlin, fourth edition, 2016.
- [16] M. Garavello and P. Goatin. The Aw-Rascle traffic model with locally constrained flow. *J. Math. Anal. Appl.*, 378(2):634–648, 2011.
- [17] M. Garavello and B. Piccoli. *Traffic flow on networks*. American Institute of Mathematical Sciences (AIMS), Springfield, MO, 2006.
- [18] J. Glimm. Solutions in the large for nonlinear hyperbolic systems of equations. *Comm. Pure Appl. Math.*, 18:697–715, 1965.
- [19] E. Godlewski and P.-A. Raviart. The numerical interface coupling of nonlinear hyperbolic systems of conservation laws. I. The scalar case. *Numer. Math.*, 97(1):81–130, 2004.
- [20] M. Gugat and M. Herty. Existence of classical solutions and feedback stabilization for the flow in gas networks. *ESAIM Control Optim. Calc. Var.*, 17(1):28–51, 2011.
- [21] M. Gugat and M. Herty. Modeling, control and numerics of gas networks. *Preprint*, 2020.
- [22] M. Gugat, M. Herty, and V. Schleper. Flow control in gas networks: exact controllability to a given demand. *Math. Methods Appl. Sci.*, 34(7):745–757, 2011.
- [23] M. Gugat, G. Leugering, A. Martin, M. Schmidt, M. Sirvent, and D. Wintergerst. MIP-based instantaneous control of mixed-integer PDE-constrained gas transport problems. *Comput. Optim. Appl.*, 70(1):267–294, 2018.
- [24] M. Gugat, G. Leugering, A. Martin, M. Schmidt, M. Sirvent, and D. Wintergerst. Towards simulation based mixed-integer optimization with differential equations. *Networks*, 72(1):60–83, 2018.

- [25] M. Herty. Modeling, simulation and optimization of gas networks with compressors. *Netw. Heterog. Media*, 2(1):81–97, 2007.
- [26] M. Herty and V. Sachers. Adjoint calculus for optimization of gas networks. *Netw. Heterog. Media*, 2(4):733–750, 2007.
- [27] C. Hös and A. R. Champneys. Grazing bifurcations and chatter in a pressure relief valve model. *Phys. D*, 241(22):2068–2076, 2012.
- [28] H. Holden and N. H. Risebro. A mathematical model of traffic flow on a network of unidirectional roads. *SIAM J. Math. Anal.*, 26(4):999–1017, 1995.
- [29] H. K. Jenssen. Blowup for systems of conservation laws. *SIAM J. Math. Anal.*, 31(4):894–908, 2000.
- [30] R. J. LeVeque. *Numerical methods for conservation laws*. Birkhäuser Verlag, Basel, 1990.
- [31] A. Martin, M. Möller, and S. Moritz. Mixed integer models for the stationary case of gas network optimization. *Math. Program.*, 105(2-3, Ser. B):563–582, 2006.
- [32] D. Modesti and S. Pirozzoli. Direct numerical simulation of supersonic pipe flow at moderate Reynolds number. *Int. J. Heat Fluid Flow*, 76:100–112, 2019.
- [33] J. D. Taylor. Numerical analysis of fast and slow transients in gas transmission networks. *Ph.D. Thesis, Heriot-Watt University*, 1997.
- [34] E. F. Toro. *Riemann solvers and numerical methods for fluid dynamics*. Springer-Verlag, Berlin, 1997. A practical introduction.
- [35] B. Ulanicki and P. Skworcow. Why PRVs tends to oscillate at low flows. *Procedia Engineer.*, 89:378–385, 2014.